

**Spectral Energetics Analysis of the
General Circulation of the Atmosphere
Using the Analytical Vertical Structure
Functions**

January 2009

Koji TERASAKI

**Spectral Energetics Analysis of the
General Circulation of the Atmosphere
Using the Analytical Vertical Structure
Functions**

A Dissertation Submitted to
the Graduate School of Life and Environmental Sciences,
the University of Tsukuba

in Partial Fulfillment of the Requirements
for the Degree of Doctor of Philosophy in Science
(Doctoral Program in Geoenvironmental Sciences)

Koji TERASAKI

CONTENTS

ABSTRACT	iii
LIST OF FIGURES	v
LIST OF TABLES	ix
CHAPTER I INTRODUCTION	1
CHAPTER II METHODOLOGY	5
2.1 Primitive Equation	5
2.2 Vertical Structure Functions	10
2.3 3D Normal Mode Functions	17
2.4 Energetics in the Vertical Wavenumber Domain	24
2.4.1 Vertical expansion of primitive equation	24
2.4.2 Kinetic energy equation	27
2.4.3 Available potential energy equation	29
2.4.4 Global energy budget equations	31
CHAPTER III DATA	33

CHAPTER IV RESULTS	34
4.1 Energetics in the Vertical Wavenumber Domain	34
4.1.1 Annual mean energetics	35
4.1.2 Seasonal mean energetics	39
4.1.3 Horizontal distribution	46
4.1.4 Difference in the vertical energy spectrum using numerical and analytical vertical structure functions	55
4.2 3D Normal Mode Energetics	59
4.2.1 Energy spectrum of the barotropic atmosphere	59
4.2.2 Energy interactions	65
 CHAPTER V DISCUSSION	 71
 CHAPTER VI CONCLUSIONS	 74
 ACKNOWLEDGEMENTS	 78
 REFERENCES	 79

ABSTRACT

In this study, the spectral energetics of the atmospheric circulation was investigated using analytical vertical structure functions. The analytical vertical structure functions can be obtained by assuming a constant static stability parameter.

According to the result of the analysis of the energy spectrum using the analytical vertical structure functions, it is found that the energy spectrum indicates a clear peak in the middle vertical modes, and the spectrum decreases monotonically at the higher order vertical modes. It is found in this study that the energy spectrum in the vertical wavenumber domain obeys -3 power of the nondimensional vertical wavenumber μ_m . The energy interactions for lower order vertical modes are consistent with that by Tanaka and Kung (1988). However, it is found from the analysis of the energy interactions that there is another energy source region in the higher order vertical modes in the zonal field. It is also found from the energy flux analysis in the vertical wavenumber domain that the atmospheric energy is converted from baroclinic component to barotropic component.

In this study, characteristics of the energy slope for the barotropic component of the atmosphere are also examined in the framework of the 3D normal mode decomposition. The energy slope of $E = mc^2$ was derived by Tanaka et al. (2004) based on the criterion of the Rossby wave breaking, where E is total energy, c is a phase speed of Rossby wave, and m is a total mass per unit area. The wave breaking occurs

when the local meridional gradient of potential vorticity q is negative, i.e., $\partial q/\partial y < 0$, somewhere in the domain. If the spectrum obeys the c^2 law, it should obey the -4 power of the zonal wavenumber n , because the phase speed c is related to the total wavenumber by $c = -\beta/k^2$, and if we assume the isotropy for zonal wind u and the meridional wind v over the range of synoptic to short waves, the energy spectrum can be expressed as a function of n instead of k .

The theoretical inference of the energy slope is examined using JRA-25 data. According to the result of the analysis, the spectral slope agrees quite well with the -4 power law of the zonal wavenumber for the barotropic component of the atmosphere. It is, however, confirmed that the spectrum obeys the -3 power law as in previous studies for the baroclinic atmosphere. It is also found that the barotropic energy spectrum obeys the saturation theory where energy cascades up, but it does not obey where energy cascades down.

According to the energetics in the vertical wavenumber domain using the analytical vertical structure functions, it is found that the available potential energy injected in the baroclinic modes converted to the kinetic energy of the same vertical scale without interacting within the vertical modes. The baroclinic kinetic energy interacts within baroclinic modes, and then they are transformed to the barotropic mode.

LIST OF FIGURES

2.1	The vertical profiles of the numerical vertical structure functions for (a) $m = 0 - 5$ and (b) $m = 17 - 22$	12
2.2	The vertical profiles of the analytical vertical structure functions for (a) $m = 0 - 5$ and (b) $m = 17 - 22$	14
4.1	The kinetic and available potential energy cycle boxes for the barotropic and baroclinic components of the Northern Hemispheric atmosphere. The units of the energy are 10^5J/m^2 , and those of the interactions term are W/m^2	37
4.2	The energy flow diagram of the atmospheric general circulation in the vertical spectral domain. The data used in this figure are the entire period of JRA-25 and JCDAS. The units of the energy are 10^3J/m^2 , and those of the interactions term are 10^{-2}W/m^2	38
4.3	As in Fig. 4.2 except for (a) DJF, (b) MAM, (c) JJA, (d) SON.	42
4.4	The horizontal distributions of barotropic (upper) and baroclinic (bot- tom) kinetic energies for Northern Hemisphere. The Units of energy are 10^5 J/m^2 . The contour interval for barotropic mode is 8×10^5 J/m^2 and for baroclinic mode is $4 \times 10^5 \text{ J/m}^2$	50

4.5	The horizontal distributions of kinetic energy for vertical mode $m = 1$ to 8. The units of energy are 10^5 J/m^2 . The contour intervals for $m = 1$ to 6 are $1 \times 10^5 \text{ J/m}^2$ and for $m = 7$ and 8 are $0.5 \times 10^5 \text{ J/m}^2$	51
4.6	The horizontal distributions of the kinetic energy generations for barotropic (upper) and baroclinic (bottom) modes in the Northern Hemisphere. The units are W/m^2 . Contour interval is 10 W/m^2	52
4.7	The horizontal distributions of kinetic energy generation for vertical mode $m = 1$ to 8. The units of energy generation are W/m^2 . The contour intervals for $m = 1$ to 6 are 2 W/m^2 and for $m = 7$ and 8 are 0.5 W/m^2	53
4.8	The horizontal distributions of the barotropic-baroclinic interactions of kinetic energy in the Northern Hemisphere. The units are W/m^2 . Contour interval is 5 W/m^2	54
4.9	The vertical energy spectrum expanded by the numerical vertical structure functions. The data period are from 1 Jan 1979 to 31 Jan 1979. The units of energy are J/m^2	57
4.10	Energy spectra of kinetic and available potential energies expanded by the analytical vertical structure functions. The data period are from 1979 to 2007. The units of energy are J/m^2	58

4.11	The total energy spectrum E_i and the energy flux associated with the nonlinear wave-wave interactions for the barotropic component in the dimensionless phase speed of the Rossby mode c_i evaluated for the 22 years of the JRA-25 during the winter DJF. Energy levels are connected by the dotted lines for the same zonal wavenumber n with the different meridional mode numbers l . The red line of the $E = ac^2$ represents the energy slope derived from the condition of the Rossby wave breaking, $\partial q/\partial y < 0$	62
4.12	The eddy energy spectrum of the Rossby and gravity modes for the barotropic component as a function of the zonal wavenumber evaluated for the 22 years of the JRA-25 during the winter DJF. Circles and square denote the energy for Rossby and gravity modes, respectively. The solid line in the figure denotes the spectral slope of -4 power derived from Eq. (4.4).	63
4.13	As in Fig. 4.12, but for the sum of the barotropic and baroclinic components of the atmosphere. The solid lines in the figure denotes the spectral slope of -3 power.	64
4.14	Energy Interactions in the wavenumber domain for (a) $m = 0 - 22$, (b) $m = 0$ and (c) $m = 1 - 22$. B: Interactions of kinetic energy, C: those of available potential energy.	68

4.15 Energy Interactions in the vertical mode domain for (a) $n = 0 - 50$, (b) $n = 0$ and (c) $n = 1 - 50$	69
4.16 Vertical energy fluxes of kinetic energy, available potential energy, and total energy as a function of the inverse of equivalent heights.	70

LIST OF TABLES

2.1	Vertical mode number, equivalent height (m), vertical wavenumber and vertical wavelength (km) of the analytical vertical structure functions used in this study.	16
2.2	The energetics terms	32
4.1	The ratio of barotropic and baroclinic kinetic energy. The units of energy are 10^5 J/m ²	41
4.2	The energy of the 3 jet regions. The units of energy are 10^6 J/m ² . . .	49

CHAPTER I

INTRODUCTION

The atmospheric energetics has been investigated since the atmospheric energy flow was discussed by Lorenz (1954) using the concept of the available potential energy. Lorenz (1954) studied the energetics of atmospheric general circulation with dividing the atmospheric data into zonal and eddy components. Saltzman (1957) expanded the energy equations into the zonal wavenumber domain and showed that the kinetic energy of the cyclone-scale waves is transformed into both the planetary waves and the short waves in terms of nonlinear wave-wave interactions. Kasahara (1976) showed a computational scheme of normal mode functions which is called Hough functions in the barotropic atmosphere. The normal modes are the solutions of the linearized primitive equations over a sphere and have been applied extensively to nonlinear normal mode initialization techniques. He applied the Hough functions to an orthonormal basis for the energy decomposition in the meridional mode domain. Since Kasahara and Puri (1981) obtained orthonormal eigensolutions to the vertical structure equation, it became possible to expand the atmospheric data into the three-dimensional harmonics of the eigensolutions. Ferdinand (1981) expanded the atmospheric data with the vertical structure functions derived by generated with empirical orthogonal function (EOF) and Bessel functions.

Tanaka (1985) and Tanaka and Kung (1988) studied the atmospheric energy spectrum and interactions expanding the atmospheric data to the three-dimensional normal mode functions. The vertical structure functions used by them were obtained by solving the vertical structure equation with a finite difference method. The numerical vertical structure functions have quite large aliasing for higher order vertical modes indicating largest amplitudes near the sea level despite that the analytical solutions indicate the largest amplitudes always in the upper atmosphere (see Sasaki and Chang 1985).

The barotropic-baroclinic interactions have been studied by many researchers (Wiin-Nielsen 1962; Nielsen and Drake 1965; Smagorinsky 1963). Wiin-Nielsen (1962) investigated the kinetic energy interactions between the vertical shear flow and the vertical mean flow. It was shown by Wiin-Nielsen for an analysis averaged over the Northern Hemisphere that the atmospheric available potential energy is released through the baroclinic flow, which acts as a catalyst, to support the motion of barotropic flow. According to their analysis, the energy conversion between shear flow and mean flow is about 30 percent of the conversion between the available potential energy and the shear flow kinetic energy.

The energy spectrum is characterized by -3 power law with respect to the horizontal wavenumber k over the synoptic to sub-synoptic scales (Wiin-Nielsen 1967; Boer and Shepherd 1983; Nastrom et al. 1984; Shepherd 1987). Using dimensional analysis, Kraichnan (1967) predicted a k^{-3} power law for 2D, isotropic and homogeneous turbulence in a downscale enstrophy cascading inertial subrange on the short-

wave side of the scale of energy injection. Basdevant et al. (1981) showed the k^{-4} spectral slope in enstrophy cascading subrange by the barotropic nondivergent model with forcing. It was shown by Tung and Orland (2003) that not only enstrophy but also energy cascade down from synoptic to meso scales. The down scale energy cascade is responsible for a $k^{-5/3}$ spectrum on the short-wave side where the energy cascade exceeds the enstrophy cascade.

Tung and Orland (2003) demonstrated that the energy injected at the synoptic scale cascades up to planetary waves and zonal motions where another dissipation exists. Contrasted to the k^{-3} law over the synoptic to subsynoptic scales, there is no appropriate theory to describe the spectral characteristics at synoptic to planetary scales because of the existence of the energy source due to baroclinic instability. Welch and Tung (1998) argued that the theory of nonlinear baroclinic adjustment (Stone 1978) is responsible to determine the spectrum over the energy source range. They introduced a breaking criterion proposed by Garcia (1991) to determine the upper bound in meridional heat flux by the disturbances. According to the criterion, a Rossby wave breaks down when a local meridional gradient of the potential vorticity is negative, i.e., $\partial q/\partial y < 0$, somewhere in the domain.

The spectral characteristic for the barotropic component in the phase speed domain was argued by Tanaka et al. (2004), by using the criterion of the $\partial q/\partial y < 0$. Using 3D normal mode energetics, they investigated the characteristics of the energy spectrum for the barotropic component (Tanaka 1985). Divergence of the shallow water system is contained mostly in the gravity modes with large phase speed c , but

it is negligible for the Rossby modes with small c because the divergence is proportional to eigenfrequency σ . Therefore, the non-divergent quasi-geostrophic model is sufficient to represent the Rossby wave breaking for the barotropic component. They derived that the energy spectrum is proportional to c^2 and also the barotropic energy spectrum of the general circulation E can be represented as $E = mc^2$. They confirmed that the theoretical inference of the slope agrees quite well with the observation.

The purposes of this study are to investigate the energetics of the atmospheric general circulation in the vertical wavenumber domain using the analytical vertical structure function, the characteristics of the energy slope in the barotropic atmosphere, and the energetics based on the 3D normal mode decomposition. Chapter II describes the methodology of this study including primitive equations, vertical structure functions, 3D normal mode functions, kinetic and available potential energy equations. Chapter III describes the data used in this study. The results of this study in Chapter IV are divided in three parts. First, the result of the energetics analysis in the vertical wavenumber domain is presented. Second, the characteristics of the energy slope in the barotropic atmosphere are described (Terasaki and Tanaka 2007a). Third, the energetics based on the 3D normal mode decomposition are described (Terasaki and Tanaka 2007b). Discussion and conclusions are given in Chapters V and VI, respectively.

CHAPTER II

METHODOLOGY

2.1 Primitive Equation

The governing equations used in this study are the primitive equations: equation of motions, thermodynamic energy equation, hydrostatic equation, equation of state, and law of mass conservation. A system of primitive equations is constituted with a spherical coordinate of longitude λ , latitude θ , nondimensional pressure $\sigma = p/p_s$ ($p_s = 1000$ hPa), and time t , where p_s is constant surface pressure:

$$\frac{\partial u}{\partial t} - 2\Omega \sin \theta v + \frac{1}{a \cos \theta} \frac{\partial \phi}{\partial \lambda} = -\mathbf{V} \cdot \nabla u - \omega \frac{\partial u}{\partial \sigma} + \frac{\tan \theta}{a} uv + F_u, \quad (2.1)$$

$$\frac{\partial v}{\partial t} + 2\Omega \sin \theta u + \frac{1}{a} \frac{\partial \phi}{\partial \theta} = -\mathbf{V} \cdot \nabla v - \omega \frac{\partial v}{\partial \sigma} - \frac{\tan \theta}{a} uv + F_v, \quad (2.2)$$

$$\frac{\partial c_p T}{\partial t} + \mathbf{V} \cdot \nabla c_p T + \omega \frac{\partial c_p T}{\partial \sigma} = \omega p_s \alpha + Q, \quad (2.3)$$

$$\frac{1}{a \cos \theta} \frac{\partial u}{\partial \lambda} + \frac{1}{a \cos \theta} \frac{\partial v \cos \theta}{\partial \theta} + \frac{\partial \omega}{\partial \sigma} = 0, \quad (2.4)$$

$$p_s \sigma \alpha = RT, \quad (2.5)$$

$$\frac{\partial \phi}{\partial \sigma} = -\frac{\alpha}{p_s}, \quad (2.6)$$

where u and v are zonal and meridional wind speed, ω is vertical p - velocity divided by constant surface pressure p_s , ϕ is geopotential, T is air temperature, a is radius

of the earth, Ω is the angular speed of the earth's rotation, c_p is the specific heat at constant pressure, α is specific volume, and R is a gas constant, respectively.

In order to obtain the conservation law of the available potential energy, we modify the thermodynamic energy equation. Dividing the air temperature T into the global mean at each pressure level and the departure from the global mean ($T = T_0 + T'$), and applying Eqs.(2.5) and (2.6) to Eq.(2.3):

$$\frac{\partial T'}{\partial t} + \mathbf{V} \cdot \nabla T' + \omega \left(\frac{\partial T'}{\partial \sigma} - \frac{RT'}{\sigma c_p} \right) + \omega \left(\frac{dT_0}{d\sigma} - \frac{RT_0}{\sigma c_p} \right) = \frac{Q}{c_p}. \quad (2.7)$$

The third term of the left hand side in Eq. (2.7) means the adiabatic change of the temperature deviation. Here, the temperature deviation is negligible compared to the global mean temperature:

$$\frac{\partial}{\partial t} \left(-\frac{\sigma^2}{R\gamma} \frac{\partial \phi'}{\partial \sigma} \right) - \frac{\sigma^2}{R\gamma} \mathbf{V} \cdot \nabla \frac{\partial \phi'}{\partial \sigma} - \frac{\omega \sigma}{\gamma} \frac{\partial}{\partial p} \left(\frac{\sigma}{R} \frac{\partial \phi'}{\partial \sigma} \right) - \omega = \frac{Q\sigma}{c_p \gamma}, \quad (2.8)$$

where the static stability parameter is (Tanaka 1985)

$$\gamma = \frac{RT_0}{c_p} - \sigma \frac{dT_0}{d\sigma}. \quad (2.9)$$

The prognostic equation of geopotential can be obtained by differentiating Eq. (2.8) with respect to nondimensional pressure σ , and applying the law of mass conservation:

$$\begin{aligned} & \frac{\partial}{\partial t} \left(-\frac{\partial}{\partial \sigma} \frac{\sigma^2}{R\gamma} \frac{\partial \phi'}{\partial \sigma} \right) + \frac{1}{a \cos \theta} \frac{\partial u}{\partial \lambda} + \frac{1}{a \cos \theta} \frac{\partial v \cos \theta}{\partial \theta} = \\ & \frac{\partial}{\partial \sigma} \left[\frac{\sigma^2}{R\gamma} \mathbf{V} \cdot \nabla \frac{\partial \phi'}{\partial \sigma} + \frac{\omega \sigma}{\gamma} \frac{\partial}{\partial \sigma} \left(\frac{\sigma}{R} \frac{\partial \phi'}{\partial \sigma} \right) \right] + \frac{\partial}{\partial \sigma} \left(\frac{Q\sigma}{c_p \gamma} \right). \end{aligned} \quad (2.10)$$

From Eqs. (2.1), (2.2) and (2.10), using a matrix notation, these primitive equations may be written as

$$\mathbf{M} \frac{\partial \mathbf{U}}{\partial t} + \mathbf{L} \mathbf{U} = \mathbf{B} + \mathbf{C} + \mathbf{F}, \quad (2.11)$$

where

$$\mathbf{U} = \begin{pmatrix} u & v & \phi' \end{pmatrix}^T \quad (2.12)$$

$$\mathbf{M} = \begin{pmatrix} 1 & 0 & 0 \\ 0 & 1 & 0 \\ 0 & 0 & -\frac{\partial}{\partial \sigma} \frac{\sigma^2}{\gamma R} \frac{\partial}{\partial \sigma} \end{pmatrix}, \quad (2.13)$$

$$\mathbf{L} = \begin{pmatrix} 0 & -2\Omega \sin \theta & \frac{1}{a \cos \theta} \frac{\partial}{\partial \lambda} \\ 2\Omega \sin \theta & 0 & \frac{1}{a} \frac{\partial}{\partial \theta} \\ \frac{1}{a \cos \theta} \frac{\partial}{\partial \lambda} & \frac{\partial(\cdot) \cos \theta}{a \cos \theta \partial \theta} & 0 \end{pmatrix}, \quad (2.14)$$

$$\mathbf{B} = \begin{pmatrix} -\mathbf{V} \cdot \nabla u - \omega \frac{\partial u}{\partial \sigma} + \frac{\tan \theta}{a} uv \\ -\mathbf{V} \cdot \nabla v - \omega \frac{\partial v}{\partial \sigma} - \frac{\tan \theta}{a} uv \\ 0 \end{pmatrix}, \quad (2.15)$$

$$\mathbf{C} = \begin{pmatrix} 0 \\ 0 \\ \frac{\partial}{\partial \sigma} \left[\frac{\sigma^2}{\gamma R} \mathbf{V} \cdot \nabla \frac{\partial \phi'}{\partial \sigma} + \frac{\omega \sigma}{\gamma} \frac{\partial}{\partial \sigma} \left(\frac{\sigma}{R} \frac{\partial \phi'}{\partial \sigma} \right) \right] \end{pmatrix}, \quad (2.16)$$

$$\mathbf{F} = \begin{pmatrix} F_u \\ F_v \\ \frac{\partial}{\partial \sigma} \left(\frac{\sigma Q}{c_p \gamma} \right) \end{pmatrix}. \quad (2.17)$$

The left-hand side of Eq. (2.11) represents linear terms with matrix operators \mathbf{M} and \mathbf{L} and the dependent variable vector \mathbf{U} . The matrix \mathbf{M} is referred to as a mass matrix which is nonsingular and positive definite under a proper boundary conditions. The right-hand side represents a nonlinear term vector \mathbf{B} and \mathbf{C} and a diabatic term vector \mathbf{F} , which includes the zonal F_u and meridional F_v components of frictional forces and a diabatic heating rate Q .

If we assume a resting atmosphere and the terms more than second order as negligible, we can derive the vertical structure equation and horizontal structure equation as follows, by the separation of variables:

$$-\frac{d}{d\sigma} \left(\sigma^2 \frac{dG_m}{d\sigma} \right) = \lambda_m G_m, \quad (2.18)$$

$$(Y_m^{-1} \mathbf{L} X_m) H_{nlm} = i \sigma_{Tnlm} H_{nlm}, \quad (2.19)$$

where G_m is the vertical structure function, the subscript m is the vertical mode number, $\lambda_m = \frac{R\gamma}{gh_m}$, $\alpha = \gamma/T_s$, p_s (=1000 hPa) and T_s (=300 K) are surface pressure and surface temperature of the reference state. σ_{Tnlm} is the eigenfrequency of the Laplace's tidal equation. It should be noticed to distinguish between nondimensional pressure σ and σ_T . The scaling matrices should be defined for each vertical index as:

$$X_m = \text{diag}(\sqrt{gh_m}, \sqrt{gh_m}, gh_m), \quad (2.20)$$

$$Y_m = \text{diag}(2\Omega\sqrt{gh_m}, 2\Omega\sqrt{gh_m}, 2\Omega), \quad (2.21)$$

where *diag* represents diagonal matrix and the entries $\sqrt{gh_m}$ is a phase speed of gravity waves in shallow water, associated with the equivalent height h_m for the vertical mode m .

2.2 Vertical Structure Functions

The vertical structure functions which are the basis functions in the vertical direction can be obtained by solving the vertical structure equation. The vertical structure equation can be obtained by assuming that the atmospheric motion is adiabatic and at rest ($\bar{u} = \bar{v} = \bar{\phi}' = 0$), and neglecting the second order and more terms.

$$-\frac{d}{d\sigma} \left(\sigma^2 \frac{dG_m}{d\sigma} \right) = \lambda_m G_m, \quad \text{for } \epsilon < \sigma < 1, \quad (2.22)$$

$$\frac{dG_m}{d\sigma} = 0, \quad \text{at } \sigma = \epsilon, \quad (2.23)$$

$$\frac{dG_m}{d\sigma} + \alpha G_m = 0, \quad \text{at } \sigma = 1. \quad (2.24)$$

According to Eq. (2.9), the static stability parameter γ is a function of mean temperature for the reference state on the nondimensional pressure σ , so the vertical structure equation can only be solved numerically. Figure 2.1 (a)-(b) show the vertical profiles of the numerical vertical structure functions by the finite difference method using the global mean climate temperature of JRA-25. Zagar et al. (submitted to Monthly Weather Review) also got the similar vertical structure functions which have a large aliasing in the higher vertical modes, because of solving the vertical structure equation numerically. The vertical mode $m = 0$ is called the barotropic mode because the values of the mode is approximately constant with no node in the vertical. The vertical mode $m = 1$ has one node in the vertical and $m = 2$ has two nodes and so on, and they are called baroclinic modes. These vertical structure functions of the lower order vertical modes have a right structure showing the largest amplitudes in the

upper atmosphere (Fig. 2.1a). However, the vertical structure functions for higher order vertical modes of $m=17$ to 22 (Fig. 2.1b) show quite large amplitudes near the sea level with almost zero values in the upper atmosphere, despite that the analytical solutions are known to have the largest amplitudes in the upper atmosphere (see Sasaki and Chang 1985).

In this study, we can get the analytical vertical structure functions by assuming that the static stability parameter γ is a constant. Since γ is a constant, the vertical structure equation becomes so-called Euler equation. Applied to a rigid top boundary condition at $\sigma = \epsilon$, the problem is reduced to the regular boundary value problem of Sturm-Liouville type. In this study the top of the atmosphere is assumed at $\sigma = 0.001$ ($p = 1$ hPa).

Under this geometric configuration, we can solve the Euler equation as a series solution (see William and Richard, 2005), and the infinite series of the vertical structure functions are represented as follows:

$$G_0(\sigma) = C_{10}\sigma^{b_{10}} + C_{20}\sigma^{b_{20}}, \quad (2.25)$$

$$G_m(\sigma) = \sigma^{-\frac{1}{2}} \{C_{1m} \cos(\mu_m \ln \sigma) + C_{2m} \sin(\mu_m \ln \sigma)\}, \quad (2.26)$$

$$b_{1m} = -\frac{1}{2} + \mu_m, \quad b_{2m} = -\frac{1}{2} - \mu_m, \quad \mu_m = \sqrt{\left| \frac{1}{4} - \lambda_m \right|}, \quad (2.27)$$

where the eigenvalues λ_m are obtained by solving the eigenvalue problem of Eq. (2.22), and the equivalent height h_m and corresponding vertical scale of each vertical mode are listed in Table 2.1. In this study, μ_m is defined as a vertical wavenumber, which has no dimension.

(a)

Numerical Vertical Structure Function

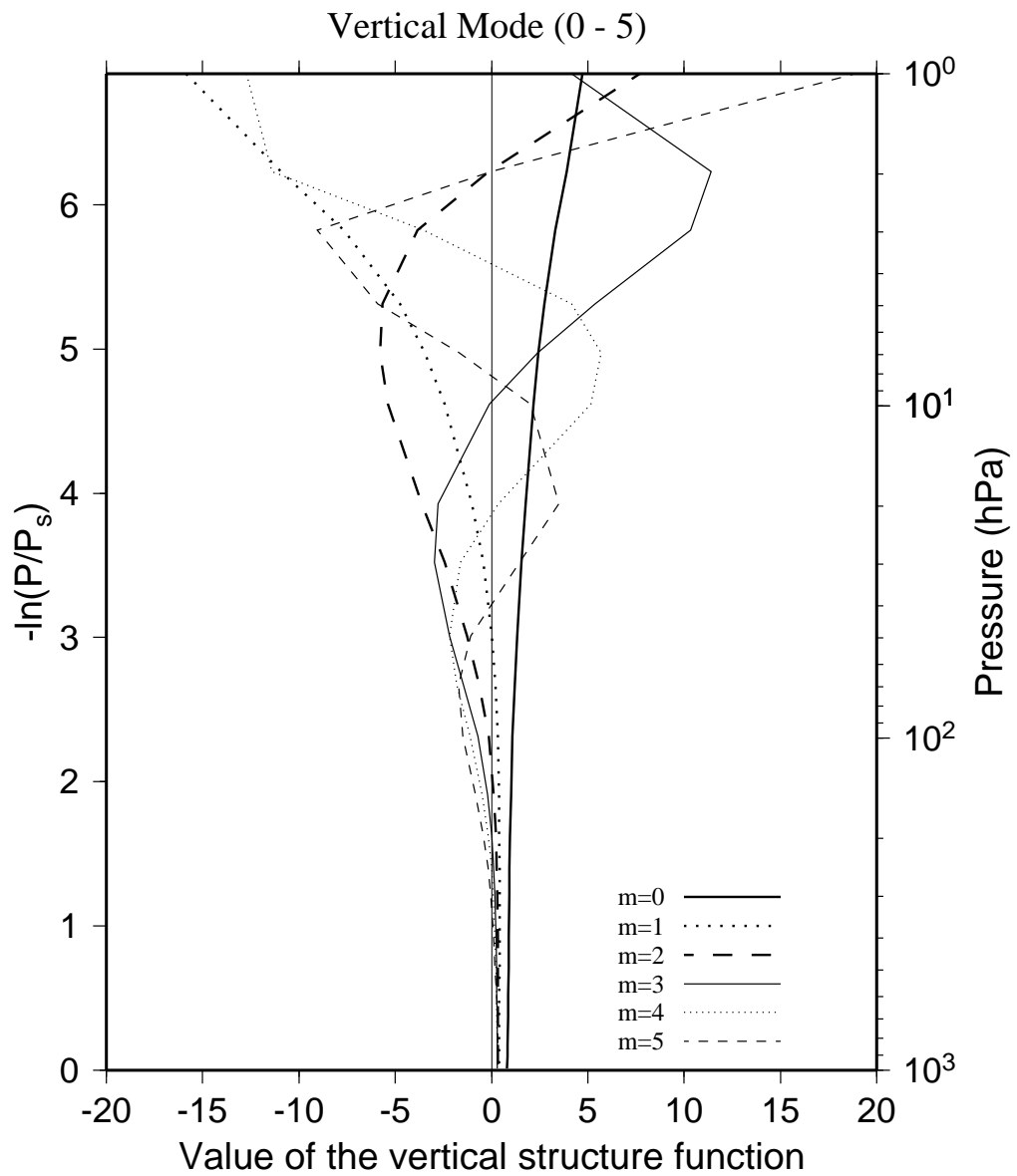


Figure 2.1. The vertical profiles of the numerical vertical structure functions for (a) $m = 0 - 5$ and (b) $m = 17 - 22$.

(b)

Numerical Vertical Structure Function

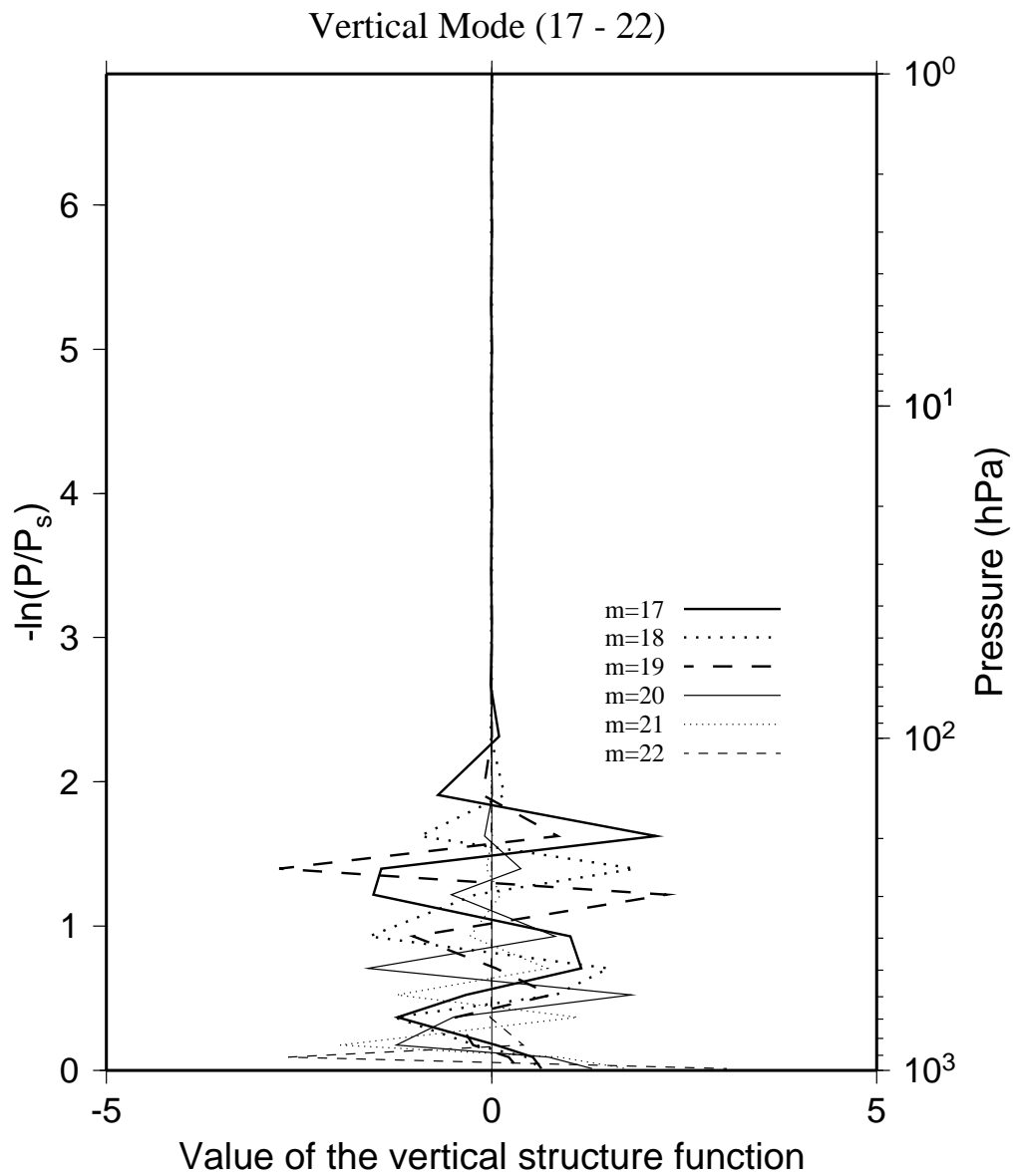


Figure 2.1. Continued.

(a)

Analytical Vertical Structure Function

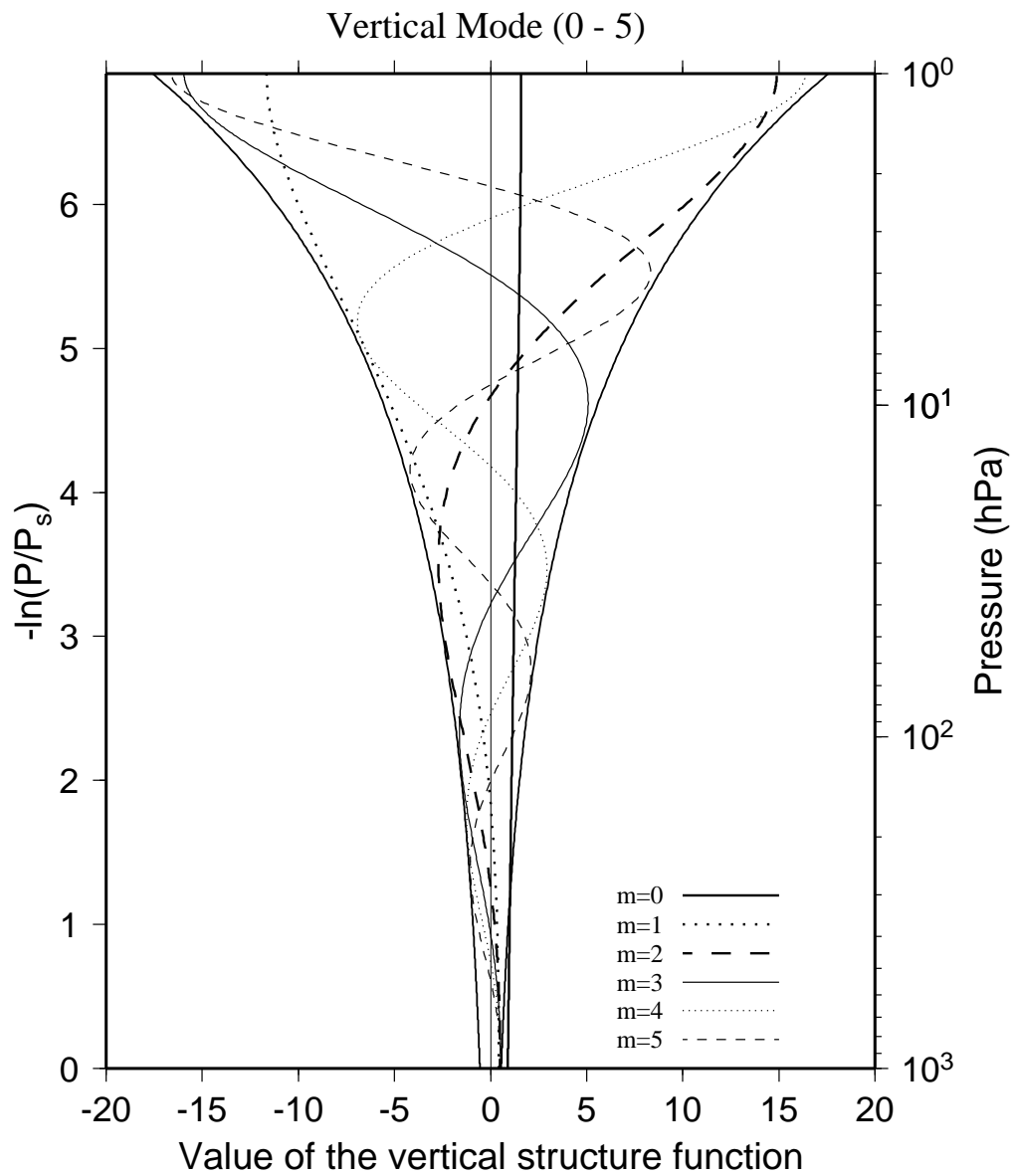


Figure 2.2. The vertical profiles of the analytical vertical structure functions for (a) $m = 0 - 5$ and (b) $m = 17 - 22$.

(b)

Analytical Vertical Structure Function

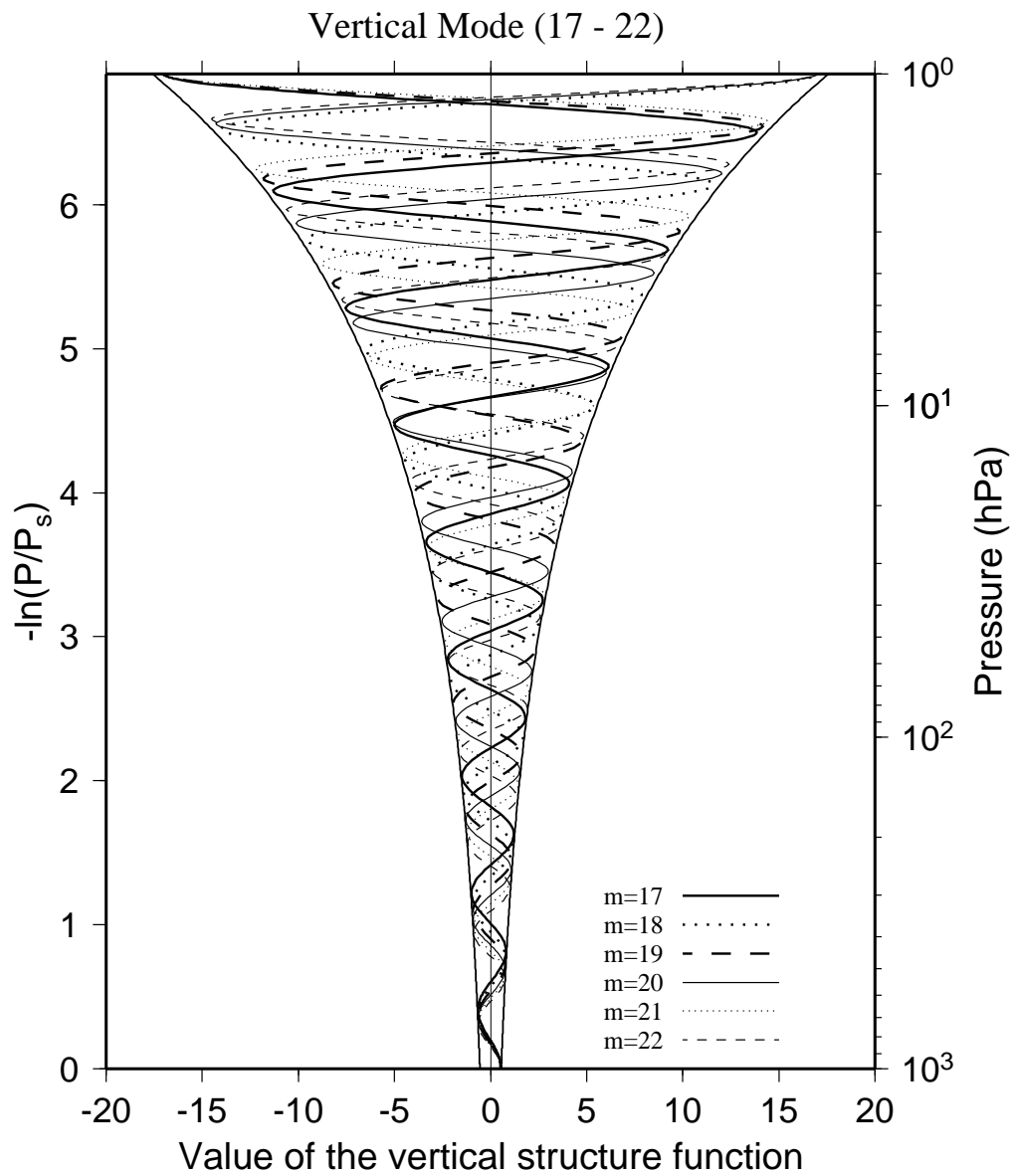


Table 2.1. Vertical mode number, equivalent height (m), vertical wavenumber and vertical wavelength (km) of the analytical vertical structure functions used in this study.

Vertical mode	Equivalent height h_m (m)	Vertical wavenumber μ_m	Vertical wavelength (km)
0	9726.6	-	-
1	1864.8	0.4709	106.75
2	800.2	0.9223	54.50
3	412.2	1.3739	36.59
4	245.7	1.8266	27.52
5	161.8	2.2801	22.05
6	114.1	2.7339	18.39
7	84.6	3.1880	15.77
8	65.2	3.6423	13.80
9	51.8	4.0966	12.27
10	42.0	4.5511	11.04
11	34.8	5.0056	10.04
12	29.3	5.4601	9.21
13	25.0	5.9147	8.50
14	21.6	6.3694	7.89
15	18.8	6.8240	7.37
16	16.6	7.2787	6.91
17	14.7	7.7333	6.50
18	13.1	8.1880	6.14
19	11.8	8.6427	5.82
20	10.6	9.0974	5.53
21	9.6	9.5521	5.26
22	8.8	10.0069	5.02

2.3 3D Normal Mode Functions

The 3-D normal mode functions are given by a tensor product of vertical structure functions (vertical normal modes, G_m) and Hough harmonics (horizontal normal modes, H_{nlm}) as $\Pi_{nlm} = G_m H_{nlm}$. It is known from Tanaka (1985) that they form a complete set and satisfy an orthonormality condition under an inner product \langle , \rangle defined as:

$$\begin{aligned} \langle \Pi_{nlm}, \Pi_{n'l'm'} \rangle &= \frac{1}{2\pi} \int_0^1 \int_{-\pi/2}^{\pi/2} \int_0^{2\pi} \Pi_{nlm} \cdot \Pi_{n'l'm'}^* \cos\theta d\lambda d\theta d\sigma \\ &= \delta_{nn'} \delta_{ll'} \delta_{mm'}, \end{aligned} \quad (2.28)$$

where the asterisk denotes the complex conjugate, the symbols δ_{ij} is the Kronecker's delta, and the surface pressure p_s is treated as a constant near the earth's surface.

In order to obtain a system of spectral primitive equations, we expand the vector U and F in 3-D normal mode functions in a resting atmosphere, $\Pi_{nlm}(\lambda, \theta, p)$:

$$U(\lambda, \theta, \sigma, t) = \sum_{nlm} w_{nlm}(t) X_m \Pi_{nlm}(\lambda, \theta, \sigma), \quad (2.29)$$

$$F(\lambda, \theta, \sigma, t) = \sum_{nlm} f_{nlm}(t) Y_m \Pi_{nlm}(\lambda, \theta, \sigma). \quad (2.30)$$

Here, the dimensionless expansion coefficients $w_{nlm}(t)$ and $f_{nlm}(t)$ are the functions of time alone. The subscripts represent zonal wavenumbers n , meridional index l , and vertical index m . They are truncated at N , L , and M , respectively.

Using the orthonormal condition (2.28) of the 3-D normal mode functions, the expansion coefficients of the state variables w_{nlm} and external forcings f_{nlm} in (2.29)

and (2.30) may be computed by the set of inverse Fourier transforms:

$$\begin{aligned} w_{nlm} &= \langle U(\lambda, \theta, \sigma, t), X_m^{-1} \Pi_{nlm}(\lambda, \theta, \sigma) \rangle, \\ f_{nlm} &= \langle F(\lambda, \theta, \sigma, t), Y_m^{-1} \Pi_{nlm}(\lambda, \theta, \sigma) \rangle. \end{aligned} \quad (2.31)$$

Applied to the same inner product for (2.11), the weak form of the primitive equation becomes

$$\langle \mathbf{M} \frac{\partial U}{\partial t} + \mathbf{L}U - N - F, Y_m^{-1} \Pi_{nlm} \rangle = 0. \quad (2.32)$$

Substituting (2.29) and (2.30) into (2.32), rearranging the time-dependent variables, and evaluating the remaining terms, we obtain a system of 3-D spectral primitive equations in terms of the spectral expansion coefficients:

$$\frac{dw_i}{d\tau} + i\sigma_{T_i} w_i = -i \sum_{jk} r_{ijk} w_j w_k + f_i, \quad i = 1, 2, 3, \dots \quad (2.33)$$

where τ is a dimensionless time scaled by $(2\Omega)^{-1}$ and r_{ijk} is the interaction coefficients for nonlinear wave-wave interactions. The triple subscripts are shortened for simplicity as $w_{nlm} = w_i$. There should be no confusion in the use of i for a subscript even though it is used for the imaginary unit.

As seen in Tanaka et al. (2004), the ratio of the nonlinear term to the linear term is referred to as a spherical Rhines ratio R_i , which characterizes the turbulence regime $R_i > 1$, and the wave regime $R_i < 1$, and the scale where $R_i = 1$ is defined as the Rhines scale C_R in this study:

$$R_i = \frac{|\sum_{jk} r_{ijk} w_j w_k|}{|\sigma_{T_i} w_i|}. \quad (2.34)$$

In order to derive (2.33) from (2.32), we first show the following relation for the linear terms.

$$\langle \mathbf{M} \frac{\partial U}{\partial t} + \mathbf{L} U, Y_m^{-1} \Pi_{nlm} \rangle = \frac{dw_i}{d\tau} + i\sigma_{Ti} w_i, \quad i = 1, 2, 3, \dots \quad (2.35)$$

The vertical differential operator \mathbf{M} may be replaced by its eigenvalue based on the relation of the vertical structure equation (2.18):

$$\mathbf{M} \Pi_i = \text{diag}(1, 1, \frac{1}{gh_i}) \Pi_i. \quad (2.36)$$

By substituting (2.29) in (2.35), using the relation in (2.19) and (2.36), we obtain

$$\begin{aligned} \sum_j \langle 2\Omega Y_j^{-1} \mathbf{M} X_j \Pi_j, \Pi_i \rangle &= \frac{dw_j}{d\tau} + \langle Y_j^{-1} \mathbf{L} X_j \Pi_j, \Pi_i \rangle w_j \\ &= \frac{dw_i}{d\tau} + i\sigma_{Ti} w_i, \end{aligned} \quad (2.37)$$

which completes the proof of (2.35).

The proof for the external forcing F in (2.32) to be transformed to f_i in (2.33) is straightforward by the relation (2.28).

Finally, we derive the specific form of the nonlinear interaction coefficients r_{ijk} in (2.33). As noted before, the 3-D normal mode function is given by the tensor products of G_m and H_{nlm} as $\Pi_{nlm} = H_{nlm} G_m$, in which the Hough harmonics are given by the tensor products of the meridional normal modes (Hough vector functions) and longitudinal normal modes (complex-valued trigonometric functions): $H_{nlm} = (U_{nlm}, -iV_{nlm}, Z_{nlm})^T e^{in\lambda}$. The computational method of the Hough vector functions $(U_{nlm}, -iV_{nlm}, Z_{nlm})^T$ are detailed by Swartrauer and Kasahara (1985), and that

of the vertical normal mode G_m by Kasahara (1984). We assume that those basis functions are already available.

By taking the inner products of the nonlinear term N and the 3-D normal mode functions, we can prove the following relation for the nonlinear interaction coefficients:

$$\langle N, Y_m^{-1} \Pi_{nlm} \rangle = -i \sum_{jk} r_{ijk} w_j w_k, \quad i = 1, 2, 3, \dots \quad (2.38)$$

The running indices i, j, k represent combinations of the 3-D wavenumbers. We need to distinguish them respectively as $n_i l_i m_i$, $n_j l_j m_j$, and $n_k l_k m_k$. Likewise, the equivalent heights and vertical structure functions are also distinguished similar way with the subscripts of i, j, k . Substituting (2.16) and (2.21) into (2.38), the inner product to be computed becomes:

$$\begin{aligned} \langle N, Y_i^{-1} \Pi_i \rangle &= \frac{1}{2\pi} \int_0^1 \int_{-\pi/2}^{\pi/2} \int_0^{2\pi} \times \\ &\times \begin{pmatrix} \frac{1}{2\Omega\sqrt{gh_i}} & U_i G_i e^{-in_i\lambda} \\ \frac{1}{2\Omega\sqrt{gh_i}} & (iV_i) G_i e^{-in_i\lambda} \\ \frac{1}{2\Omega} & Z_i G_i e^{-in_i\lambda} \end{pmatrix}^T \begin{pmatrix} -V \cdot \nabla u - \omega \frac{\partial u}{\partial \sigma} + \frac{\tan \theta}{a} uv \\ -V \cdot \nabla v - \omega \frac{\partial v}{\partial \sigma} - \frac{\tan \theta}{a} uv \\ \frac{\partial}{\partial \sigma} [V \cdot \nabla (\frac{\sigma^2}{R\gamma} \frac{\partial \phi'}{\partial \sigma}) + \omega \sigma \frac{\partial}{\partial \sigma} (\frac{\sigma}{R\gamma} \frac{\partial \phi'}{\partial \sigma})] \end{pmatrix} \cos \theta d\lambda d\theta d\sigma. \end{aligned} \quad (2.39)$$

It is recognized that the nonlinear terms are at most the second order nonlinearity of the state variables. Using (2.29) we substitute the following expansion of the state variables in the nonlinear terms of (2.39):

$$\begin{pmatrix} u \\ v \\ \phi' \end{pmatrix} = \sum_i w_i \begin{pmatrix} \sqrt{gh_i} & U_i \\ \sqrt{gh_i} & (-iV_i) \\ gh_i & Z_i \end{pmatrix} G_i e^{in_i\lambda}. \quad (2.40)$$

The vertical p-velocity ω may be expanded as the next form based on the continuity equation:

$$\omega = \sum_i w_i 2\Omega \int_0^\sigma G_i d\sigma (-i\sigma_i Z_i) e^{in_i\lambda}. \quad (2.41)$$

The vertical integral in (2.41) can be replaced by the first order derivative derived from the integral of (2.18) as:

$$\int_0^\sigma G_i d\sigma = -\frac{gh_i}{R\gamma} \sigma^2 \frac{dG_i}{d\sigma}. \quad (2.42)$$

Moreover, the second order vertical derivative in (2.39) can be replaced by the first order derivative derived from (2.18) as:

$$-\sigma \frac{d}{d\sigma} \frac{\sigma}{R\gamma} \frac{dG_i}{d\sigma} = \frac{\sigma}{R\gamma} \frac{dG_i}{d\sigma} + \frac{G_i}{gh_i}. \quad (2.43)$$

With those preparations, the final form of the computation for the nonlinear interaction coefficients is summarized as the volume integral of the triple products of the normal mode functions:

$$\begin{aligned} \langle N, Y_i^{-1} \Pi_i \rangle &= -i \sum_j \sum_k w_j w_k \frac{1}{2\pi} \int_0^1 \int_{-\pi/2}^{\pi/2} \int_0^{2\pi} \\ &\begin{pmatrix} U_i \\ V_i \\ Z_i \end{pmatrix}^T \begin{pmatrix} P_1 \left(\frac{n_k U_k}{\cos \theta} + \tan \theta V_k \right) & -P_1 \frac{dU_k}{d\theta} & P_2 U_k \\ P_1 \left(\frac{n_k V_k}{\cos \theta} + \tan \theta U_k \right) & -P_1 \frac{dV_k}{d\theta} & P_2 V_k \\ P_3 \frac{n_k Z_k}{\cos \theta} & -P_3 \frac{dZ_k}{d\theta} & -P_4 Z_k \end{pmatrix} \begin{pmatrix} U_j \\ V_j \\ \sigma_j Z_j \end{pmatrix} \\ &e^{i(-n_i+n_j+n_k)\lambda} \cos \theta d\lambda d\theta d\sigma. \end{aligned} \quad (2.44)$$

Here, the triple products of the vertical structure functions are combined with the scaling parameters as:

$$P_1 = \frac{\sqrt{gh_j} \sqrt{gh_k}}{2\Omega \alpha \sqrt{gh_i}} G_i G_j G_k,$$

$$\begin{aligned}
P_2 &= \frac{\sqrt{gh_k}gh_j}{\sqrt{gh_i}R\gamma}\sigma^2G_i\frac{dG_j}{d\sigma}\frac{dG_k}{d\sigma}, \\
P_3 &= \frac{\sqrt{gh_j}}{2\Omega a}G_iG_jG_k - \frac{\sqrt{gh_j}gh_k}{2\Omega aR\gamma}\sigma^2G_i\frac{dG_j}{d\sigma}\frac{dG_k}{d\sigma}, \\
P_4 &= G_iG_jG_k + \frac{gh_k}{R\gamma}\sigma G_iG_j\frac{dG_k}{d\sigma} + \frac{gh_j}{R\gamma}\sigma G_i\frac{dG_j}{d\sigma}G_k \\
&\quad + \left(\frac{gh_k}{R\gamma} - 1\right)\frac{gh_j}{R\gamma}\sigma^2G_i\frac{dG_j}{d\sigma}\frac{dG_k}{d\sigma}, \tag{2.45}
\end{aligned}$$

which completes the description of the real-valued nonlinear interaction coefficients r_{ijk} , represented by the volume integral in (2.44). The analytical derivative of the vertical structure function is available as from Eqs. (2.25) and (2.26).

As shown in (2.44), the nonlinear interactions are non-zero only when the zonal wavenumbers satisfy the relation $n_i = n_j + n_k$. In (2.44), there are many first derivatives of the normal modes which are obtainable analytically when these are evaluated in terms of a series expansion with the Associated Legendre functions. Hence, the computations for r_{ijk} are all analytical except for the volume integrals by means of the Gaussian quadrature which is exact under the specified truncations of the Legendre polynomials. It is worth noting that the spectral primitive equation (2.33) is as accurate as the original one in (2.11) with approximately 1% in error for the dynamics part.

The energy of the normal mode is defined as the square of the absolute value of the complex expansion coefficient w_{nlm} , multiplied by a dimensional factor chosen so that the energy is expressed in J/m²:

$$E_{0lm} = \frac{1}{4}p_s h_m |w_{0lm}|^2, \tag{2.46}$$

$$E_{nlm} = \frac{1}{2}p_s h_m |w_{nlm}|^2. \tag{2.47}$$

In order to obtain the energy balance equations for normal modes, Eqs. (2.46) and (2.47) are differentiated with respect to time τ . Substituting (2.33) into the time derivatives of w_{nlm} , we obtain finally:

$$\frac{dE_{nlm}}{dt} = B_{nlm} + C_{nlm} + D_{nlm}, \quad (2.48)$$

where

$$B_{nlm} = p_s \Omega h_m (w_{nlm}^* b_{nlm} + w_{nlm} b_{nlm}^*), \quad (2.49)$$

$$C_{nlm} = p_s \Omega h_m (w_{nlm}^* c_{nlm} + w_{nlm} c_{nlm}^*), \quad (2.50)$$

$$D_{nlm} = p_s \Omega h_m (w_{nlm}^* d_{nlm} + w_{nlm} d_{nlm}^*). \quad (2.51)$$

According to (2.48), the time change of the energy is caused by the three terms which appear in the right hand side of (2.48). B_{nlm} and C_{nlm} are respectively associated with the nonlinear mode-mode interactions of kinetic and available potential energies, and D_{nlm} represents an energy source and sink due to the diabatic process and dissipation.

2.4 Energetics in the Vertical Wavenumber Domain

2.4.1 Vertical expansion of primitive equation

In this study, the energetics of the atmospheric general circulation is analyzed in the vertical spectral domain. The kinetic energy equation in the vertical spectral domain can be obtained by expanding the equation of motions (Eqs. 2.1 and 2.2) using the vertical structure functions and multiplying the wind vector. Also the available potential energy equation can be obtained by expanding Eq. (2.10) using vertical structure functions. Expanding the primitive equations by the vertical structure functions and applying the boundary conditions (Eqs. 2.23 and 2.24), the primitive equations in the vertical spectral domain are represented as follows:

$$\begin{aligned} \frac{\partial U_m}{\partial t} = - \sum_{l,n} \left[\frac{r_{lnm}}{a \cos \theta} U_l \frac{\partial U_n}{\partial \lambda} + \frac{r_{lnm}}{a} V_l \frac{\partial U_n}{\partial \theta} + r_{ln'm} \Omega_l U_n - \frac{\tan \theta}{a} r_{lnm} U_l V_n \right] \\ + f V_m - \frac{1}{a \cos \theta} \frac{\partial A_m}{\partial \lambda} - X_m, \end{aligned} \quad (2.52)$$

$$\begin{aligned} \frac{\partial V_m}{\partial t} = - \sum_{l,n} \left[\frac{r_{lnm}}{a \cos \theta} U_l \frac{\partial V_n}{\partial \lambda} + \frac{r_{lnm}}{a} V_l \frac{\partial V_n}{\partial \theta} + r_{ln'm} \Omega_l V_n - \frac{\tan \theta}{a} r_{lnm} U_l U_n \right] \\ - f U_m - \frac{1}{a} \frac{\partial A_m}{\partial \theta} - Y_m, \end{aligned} \quad (2.53)$$

$$\begin{aligned}
\frac{1}{h_m} \frac{\partial A_m}{\partial t} &= \sum_{l,n} \frac{g}{R\gamma} r_{\sigma^2 \nu' n' m} \left[\frac{1}{a \cos \theta} U_l \frac{\partial A_n}{\partial \lambda} + \frac{1}{a} V_l \frac{\partial A_n}{\partial \theta} \right] \\
&+ \sum_{l,n} \frac{g}{R\gamma} (r_{\sigma l n' m'} + \lambda_n r_{l n m'}) \Omega_l A_n \\
&- \frac{1}{a \cos \theta} \frac{\partial U_m}{\partial \lambda} - \frac{1}{a} \frac{\partial V_m}{\partial \theta} + \frac{\tan \theta}{a} V_m \\
&+ \frac{1}{C_p \gamma} (H_m + \sum_n H_n r_{\sigma n' m}),
\end{aligned} \tag{2.54}$$

$$\frac{1}{a \cos \theta} \frac{\partial U_m}{\partial \lambda} - \frac{\tan \theta}{a} V_m + \frac{1}{a} \frac{\partial V_m}{\partial \theta} + \sum_n \Omega_n r_{n' m} = 0, \tag{2.55}$$

$$g \sum_n r_{n' m} A_n = \frac{\alpha_m}{p_s}, \tag{2.56}$$

where U , V , Ω , A , and α are the vertical expansion coefficients of horizontal wind speeds u and v , vertical p -velocity ω , geopotential ϕ , and specific volume α , respectively. The subscripts l, n , and m are the vertical mode number. In Eqs (2.52) - (2.56), r is an integration of the triple or double products of the vertical structure function G :

$$r_{l n m} = \int_{\epsilon}^1 G_l G_n G_m d\sigma, \tag{2.57}$$

$$r_{l n' m} = \int_{\epsilon}^1 G_l \frac{\partial G_n}{\partial \sigma} G_m d\sigma, \tag{2.58}$$

$$r_{\sigma^2 \nu' n' m} = \int_{\epsilon}^1 \sigma^2 \frac{\partial G_l}{\partial \sigma} \frac{\partial G_n}{\partial \sigma} G_m d\sigma, \tag{2.59}$$

$$r_{\sigma l n' m'} = \int_{\epsilon}^1 \sigma G_l \frac{\partial G_n}{\partial \sigma} \frac{\partial G_m}{\partial \sigma} d\sigma, \tag{2.60}$$

$$r_{l n m'} = \int_{\epsilon}^1 G_l G_n \frac{\partial G_m}{\partial \sigma} d\sigma, \tag{2.61}$$

$$r_{\sigma n' m} = \int_{\epsilon}^1 \sigma \frac{\partial G_n}{\partial \sigma} G_m d\sigma, \tag{2.62}$$

$$r_{n' m} = \int_{\epsilon}^1 \frac{\partial G_n}{\partial \sigma} G_m d\sigma. \tag{2.63}$$

Since σ is a nondimensional pressure, these nonlinear coefficients r become nondimensional. The nonlinear coefficients r can be derived analytically by using the boundary conditions, because these are the double or triple products of the vertical structure functions G .

$$r_{lnm} = \sum_{i,j,k=1}^2 \frac{C_{il}C_{jn}C_{km}}{b_{il} + b_{jn} + b_{km} + 1.0} (1.0 - \epsilon^{b_{il}+b_{jn}+b_{km}+1.0}), \quad (2.64)$$

$$r_{ln'm} = \sum_{i,j,k=1}^2 \frac{C_{il}C_{jn}C_{km}b_{jn}}{b_{il} + b_{jn} + b_{km}} (1.0 - \epsilon^{b_{il}+b_{jn}+b_{km}}), \quad (2.65)$$

$$r_{\sigma^2 l'n'm} = \sum_{i,j,k=1}^2 \frac{C_{il}C_{jn}C_{km}b_{jn}b_{il}}{b_{il} + b_{jn} + b_{km} + 1.0} (1.0 - \epsilon^{b_{il}+b_{jn}+b_{km}}), \quad (2.66)$$

$$r_{\sigma l'n'm'} = \sum_{i,j,k=1}^2 \frac{C_{il}C_{jn}C_{km}b_{km}b_{jn}}{b_{il} + b_{jn} + b_{km}} (1.0 - \epsilon^{b_{il}+b_{jn}+b_{km}}), \quad (2.67)$$

$$r_{lnm'} = \sum_{i,j,k=1}^2 \frac{C_{il}C_{jn}C_{km}b_{km}}{b_{il} + b_{jn} + b_{km}} (1.0 - \epsilon^{b_{il}+b_{jn}+b_{km}}). \quad (2.68)$$

2.4.2 Kinetic energy equation

The kinetic energy per unit area is described as follows:

$$K = \frac{p_s}{g} \int_{\epsilon}^1 \frac{u^2 + v^2}{2} d\sigma, \quad (2.69)$$

where K is a kinetic energy, and the units of K are J/m². Expanding u and v with the vertical structure functions and using the orthonormality of the vertical structure functions,

$$\begin{aligned} K &= \frac{p_s}{g} \int_{\epsilon}^1 \frac{1}{2} \left[\sum_m U_m G_m \sum_n U_n G_n + \sum_m V_m G_m \sum_n V_n G_n \right] d\sigma, \\ &= \frac{p_s}{g} \sum_m \sum_n \frac{U_m U_n + V_m V_n}{2} \int_{\epsilon}^1 G_m G_n d\sigma, \\ &= \frac{p_s}{g} \sum_m \frac{U_m^2 + V_m^2}{2}, \\ &= \sum_m K_m, \end{aligned} \quad (2.70)$$

where

$$K_m = \frac{p_s}{g} \frac{U_m^2 + V_m^2}{2}, \quad (2.71)$$

and K_m is the kinetic energy of each vertical mode. Differentiating Eq. (2.71) with respect to time t , kinetic energy equation in the vertical wavenumber domain can be obtained,

$$\begin{aligned}
\frac{\partial K_m}{\partial t} &= \frac{p_s}{g} \left(U_m \frac{\partial U_m}{\partial t} + V_m \frac{\partial V_m}{\partial t} \right) \\
&= -\frac{p_s}{g} \sum_{l,n} \left[\frac{r_{lnm}}{a \cos \theta} \left(U_m U_l \frac{\partial U_n}{\partial \lambda} + V_m U_l \frac{\partial V_n}{\partial \lambda} \right) \right. \\
&\quad + \frac{r_{lnm}}{a} \left(U_m V_l \frac{\partial U_n}{\partial \theta} + V_m V_l \frac{\partial V_n}{\partial \theta} \right) - \frac{\tan \theta}{a} r_{lnm} \left(U_m U_l V_n - V_m U_l U_n \right) \\
&\quad \left. + r_{ln'm} \left(U_m \Omega_l U_n - V_m U_l V_n \right) \right] \\
&\quad - \frac{p_s}{g} \frac{1}{a \cos \theta} U_m \frac{\partial A_m}{\partial \lambda} - \frac{p_s}{g} \frac{1}{a} V_m \frac{\partial A_m}{\partial \theta} - D_m. \tag{2.72}
\end{aligned}$$

In this kinetic energy equation, the first to fourth terms of the right hand side show the kinetic energy interactions among baroclinic-baroclinic and barotropic-baroclinic components, the fifth and sixth terms show the generation of the kinetic energy, which is converted from available potential energy, and last term shows the dissipation of the kinetic energy, respectively.

2.4.3 Available potential energy equation

Available potential energy is represented using the geopotential ϕ' as follows:

$$P = \frac{p_s}{g} \int_{\epsilon}^1 \frac{\sigma^2}{2R\gamma} \left(\frac{\partial \phi'}{\partial \sigma} \right)^2 d\sigma. \quad (2.73)$$

Applying the chain rule to the right hand side in Eq. (2.73), expanding the geopotential deviation ϕ' with the vertical structure functions, and

$$\begin{aligned} P &= \frac{p_s}{g} \int_{\epsilon}^1 \frac{1}{2} \frac{\partial}{\partial \sigma} \left(\frac{\sigma^2}{R\gamma} \phi' \frac{\partial \phi'}{\partial \sigma} \right) - \frac{\phi'}{2} \frac{\partial}{\partial \sigma} \left(\frac{\sigma^2}{R\gamma} \frac{\partial \phi'}{\partial \sigma} \right) d\sigma, \\ &= \frac{p_s^2}{2R\gamma g} \phi'_s \frac{\partial \phi'_s}{\partial \sigma} - \frac{1}{2g} \sum_n \sum_m A_n A_m \int_{\epsilon}^1 G_n \frac{\partial}{\partial \sigma} \left(\frac{\sigma^2}{R\gamma} \frac{\partial G_m}{\partial \sigma} \right) d\sigma, \\ &= \frac{p_s^2}{2R\gamma g} \phi'_s \frac{\partial \phi'_s}{\partial \sigma} - \frac{1}{2g} \sum_n \sum_m A_n A_m \int_{\epsilon}^1 G_n \frac{G_m}{gh_m} d\sigma, \\ &= \frac{p_s^2}{2R\gamma g} \phi'_s \frac{\partial \phi'_s}{\partial \sigma} + \sum_m P_m, \end{aligned} \quad (2.74)$$

where

$$P_m = \frac{p_s}{2g^2 h_m} A_m^2, \quad (2.75)$$

where ϕ'_s denotes the surface geopotential. P is available potential energy and P_m is the available potential energy of each vertical mode, and the unit is J/m^2 . Differentiating Eq. (2.75) with respect to time t , we can obtain the available potential energy equation:

$$\frac{\partial P_m}{\partial t} = \frac{p_s}{g^2 h_m} A_m \frac{\partial A_m}{\partial t}. \quad (2.76)$$

Substituting Eq. (2.54) to Eq. (2.76), we can obtain the available potential energy equation in the vertical spectral domain:

$$\begin{aligned}
\frac{\partial P_m}{\partial t} = & \sum_{l,n} \frac{p_s}{g} \frac{1}{R\gamma} r_{\sigma^2 l' n' m} \left[\frac{A_m}{a \cos \theta} U_l \frac{\partial A_n}{\partial \lambda} + \frac{A_m}{a} V_l \frac{\partial A_n}{\partial \theta} \right] \\
& + \sum_{l,n} \frac{p_s}{g} \frac{1}{R\gamma} (r_{\sigma l n' m'} + \lambda_n r_{l n m'}) A_m \Omega_l A_n \\
& + \frac{p_s}{g} \frac{U_m}{a \cos \theta} \frac{\partial A_m}{\partial \lambda} + \frac{p_s}{g} \frac{V_m}{a} \frac{\partial A_m}{\partial \theta} \\
& + \frac{p_s}{C_p \gamma} A_m \left(H_m + \sum_n r_{\sigma n' m} H_n \right), \tag{2.77}
\end{aligned}$$

where the first two lines show the available potential energy interactions within the baroclinic-baroclinic and barotropic-baroclinic components of the atmosphere, and the third line shows the conversion to the same scale of the kinetic energy, and the last line shows the generation of the available potential energy or dissipation due to the radiative cooling. In this study, the last term is evaluated as a residual from the other terms.

2.4.4 Global energy budget equations

In order to obtain the energy budget equations, we summarize the kinetic energy and available potential energy equations.

$$\frac{\partial K_m}{\partial t} = -M(m) + L(m) + C(m) - D(m), \quad (2.78)$$

$$\frac{\partial K_0}{\partial t} = \sum_{m=1}^M M(m) + C(0) - D(0), \quad (2.79)$$

$$\frac{\partial P_m}{\partial t} = R(m) + S(m) - C(m) + G(m), \quad (2.80)$$

$$\frac{\partial P_0}{\partial t} = -\sum_{m=1}^M R(m) - C(0) + G(0). \quad (2.81)$$

Eqs. (2.78) - (2.81) are the energy budget equations for the baroclinic kinetic energy, the barotropic kinetic energy, the baroclinic available potential energy, and the barotropic available potential energy, respectively. The details about each term in these equations are described in Table 2.2. The atmospheric energy flows in the vertical spectral domain can be examined by calculating these terms.

Table 2.2. The energetics terms

$C(m)$	$-\frac{p_s}{g} \left(\frac{1}{a \cos \theta} U_m \frac{\partial A_m}{\partial \lambda} + \frac{1}{a} V_m \frac{\partial A_m}{\partial \theta} \right)$	Kinetic energy generation
$L(m)$	$-\frac{p_s}{g} \sum_{l,n \neq 0} \left[\frac{r_{lmm}}{a \cos \theta} (U_m U_l \frac{\partial U_n}{\partial \lambda} + V_m U_l \frac{\partial V_n}{\partial \lambda}) + V_m U_l \frac{\partial U_n}{\partial \theta} + V_m V_l \frac{\partial V_n}{\partial \theta} \right] -$	Baroclinic-baroclinic interactions of kinetic energy.
$M(m)$	$\frac{\tan \theta}{a} r_{lmm} (U_m U_l V_n - V_m U_l U_n) \left[\frac{r_{0mm}}{a \cos \theta} (U_m U_0 \frac{\partial U_n}{\partial \lambda} + V_m U_0 \frac{\partial V_n}{\partial \lambda}) + \frac{r_{0mm}}{a} (U_m V_0 \frac{\partial U_n}{\partial \theta} + V_m V_0 \frac{\partial V_n}{\partial \theta}) - \right. \\ \left. \frac{\tan \theta}{a} r_{0mm} (U_m U_0 V_n - V_m U_0 U_n) \right] - \frac{p_s}{g} \sum_{l=1}^L \left[\frac{r_{l0m}}{a \cos \theta} (U_m U_l \frac{\partial U_0}{\partial \lambda} + V_m U_l \frac{\partial V_0}{\partial \lambda}) + \right. \\ \left. \frac{r_{l0m}}{a} (U_m V_l \frac{\partial U_0}{\partial \theta} + V_m V_l \frac{\partial V_0}{\partial \theta}) - \frac{\tan \theta}{a} r_{l0m} (U_m U_l V_0 - V_m U_l U_0) \right]$	Barotropic-baroclinic interactions of kinetic energy for baroclinic mode.
$M(0)$	$-\sum_{m=1}^M M(m)$	Barotropic-baroclinic interactions of kinetic energy for barotropic mode.
$S(m)$	$\frac{p_s}{g} \frac{1}{R\gamma} \sum_{l,n \neq 0} \left[r_{\sigma^2 l' n' m} \left(\frac{A_m}{a \cos \theta} U_l \frac{\partial A_n}{\partial \lambda} + \frac{A_m}{a} V_l \frac{\partial A_n}{\partial \theta} \right) + (r_{\sigma l' m'} + \lambda_n r_{l m m'}) A_m \Omega_l A_n \right]$	Baroclinic-baroclinic interactions of available potential energy.
$R(m)$	$\frac{p_s}{g} \frac{1}{R\gamma} \sum_{n=0}^N \left[r_{\sigma^2 0' n' m} \left(\frac{A_m}{a \cos \theta} U_0 \frac{\partial A_n}{\partial \lambda} + \frac{A_m}{a} V_0 \frac{\partial A_n}{\partial \theta} \right) + (r_{\sigma 0 n' m'} + \right. \\ \left. \lambda_n r_{0 n m'} A_m \Omega_0 A_n \right] + \frac{p_s}{g} \frac{1}{R\gamma} \sum_{l=1}^L \left[r_{\sigma^2 l' 0' m} \left(\frac{A_m}{a \cos \theta} U_l \frac{\partial A_0}{\partial \lambda} + \frac{A_m}{a} V_l \frac{\partial A_0}{\partial \theta} \right) + (r_{\sigma l' 0' m'} + \right. \\ \left. \lambda_n r_{l 0 m'} A_m \Omega_l A_0 \right]$	Barotropic-baroclinic interactions of available potential energy for baroclinic modes.
$R(0)$	$-\sum_{m=1}^M R(m)$	Barotropic-baroclinic interactions of available potential energy for barotropic mode.

CHAPTER III

DATA

In this study, JRA-25 (Japanese Re-Analysis 25 years) and JCDAS (JMA Climate Data Assimilation System) (Onogi et al. 2007) are used. JRA-25 is the first reanalysis in Japan conducted by JMA and CRIEPI (Central Research Institute of Electric Power Industry). The reanalysis period is from January 1979 to December 2004. The global model resolution is T106L40 (the model top is 0.4 hPa). JCDAS is the real-time reanalysis, which is taken over the same system as JRA-25 and the data assimilation cycle is extended up to the present. The data used in this study are four-times daily (00, 06, 12, and 18 UTC) JRA-25 and JCDAS (Onogi et al. 2007). The data contain meteorological variables of horizontal wind u , v , vertical p -velocity, temperature, and geopotential ϕ , defined at every 2.5° longitude by 2.5° latitude grid points over 23 mandatory vertical levels from 1000 to 0.4 hPa. The atmospheric data at 0.4 hPa doesn't use, because the boundary condition for top of the atmosphere is set to 1.0 hPa. The data are interpolated on the 46 Gaussian vertical levels in the $\log(p/p_s)$ coordinate by cubic spline method.

CHAPTER IV

RESULTS

4.1 Energetics in the Vertical Wavenumber Domain

In this section, the results of the energetics analysis in the vertical wavenumber domain are introduced. The energy interactions in the vertical wavenumber domain can be investigated by expanding the primitive equation with the vertical structure functions. Also, the energy flow between the barotropic and baroclinic motion can be examined by summing up the energetics terms of all baroclinic modes.

4.1.1 Annual mean energetics

Figure 4.1 shows energy flow of kinetic energy and available potential energy between barotropic and baroclinic component. The energy source of the atmospheric general circulation is basically only the solar heating. It is injected as baroclinic available potential energy by the differential heating between equator and polar regions, and its magnitude is 2.28 W/m^2 . The baroclinic conversion, which is the energy conversion from available potential energy to kinetic energy by the baroclinic instability, is 2.10 W/m^2 . A part of this baroclinic kinetic energy is dissipated by the viscosity or friction, and the amount of the dissipation is 1.07 W/m^2 . Another part of baroclinic kinetic energy is transformed to the barotropic motion. Finally, the barotropic kinetic energy is dissipated by the viscosity or friction.

Figure 4.2 shows the kinetic energy and available potential energy flows in the vertical wavenumber domain. The similar analysis in the zonal wavenumber domain, which the Fourier expansion is used for basis function, is performed by Saltzman (1985) and Tanaka and Kung (1988). It is found in this study that the generation of the baroclinic available potential energy is widely distributed to the higher order vertical modes, while the maximum injection is at the lower order vertical modes around $m = 4$. The largest energy source is 0.53 W/m^2 in the vertical mode $m = 4$. The sum of the energy injection from the vertical modes $m = 2$ to 8 is 2.08 W/m^2 . The barotropic available potential energy actually should be zero if the barotropic mode means strictly vertical mean. But the vertical structure function of vertical

mode $m = 0$ doesn't have a constant value, so the available potential energy of the barotropic mode has a nonzero value. It is found that the interactions of the available potential energy between baroclinic-baroclinic and barotropic-baroclinic are very small compared to those of the kinetic energy. The baroclinic available potential energy is directly converted to the same scale of the kinetic energy with interacting little among them. The energy conversion of each vertical mode is mostly same with the energy injection of corresponding vertical mode. Most of the baroclinic conversions have positive values except for the barotropic mode ($m = 0$) and the first baroclinic modes ($m = 1$). It is found that the baroclinic kinetic energy interacts within baroclinic modes, and then they are transformed to the barotropic mode. The energy interactions in higher order vertical modes have a zigzag distribution. This is caused by the artificial rigid upper boundary where the vertical structure function in upper atmosphere has a large amplitude.

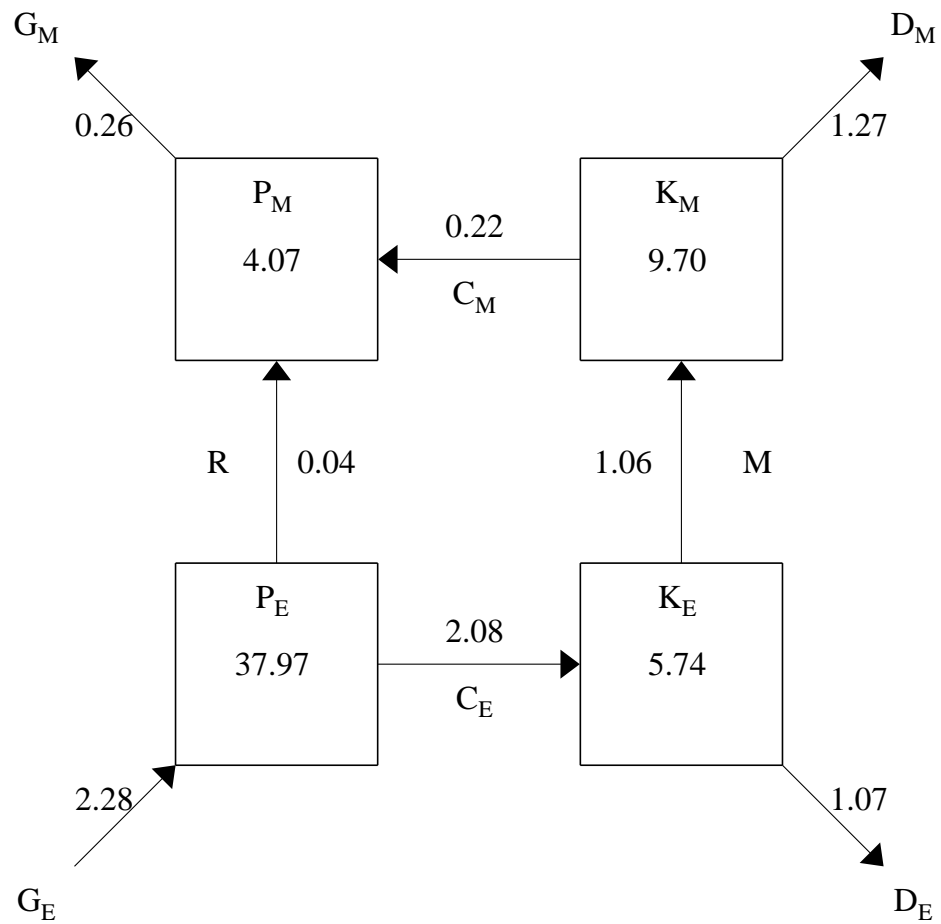


Figure 4.1. The kinetic and available potential energy cycle boxes for the barotropic and baroclinic components of the Northern Hemispheric atmosphere. The units of the energy are 10^5 J/m^2 , and those of the interactions term are W/m^2 .

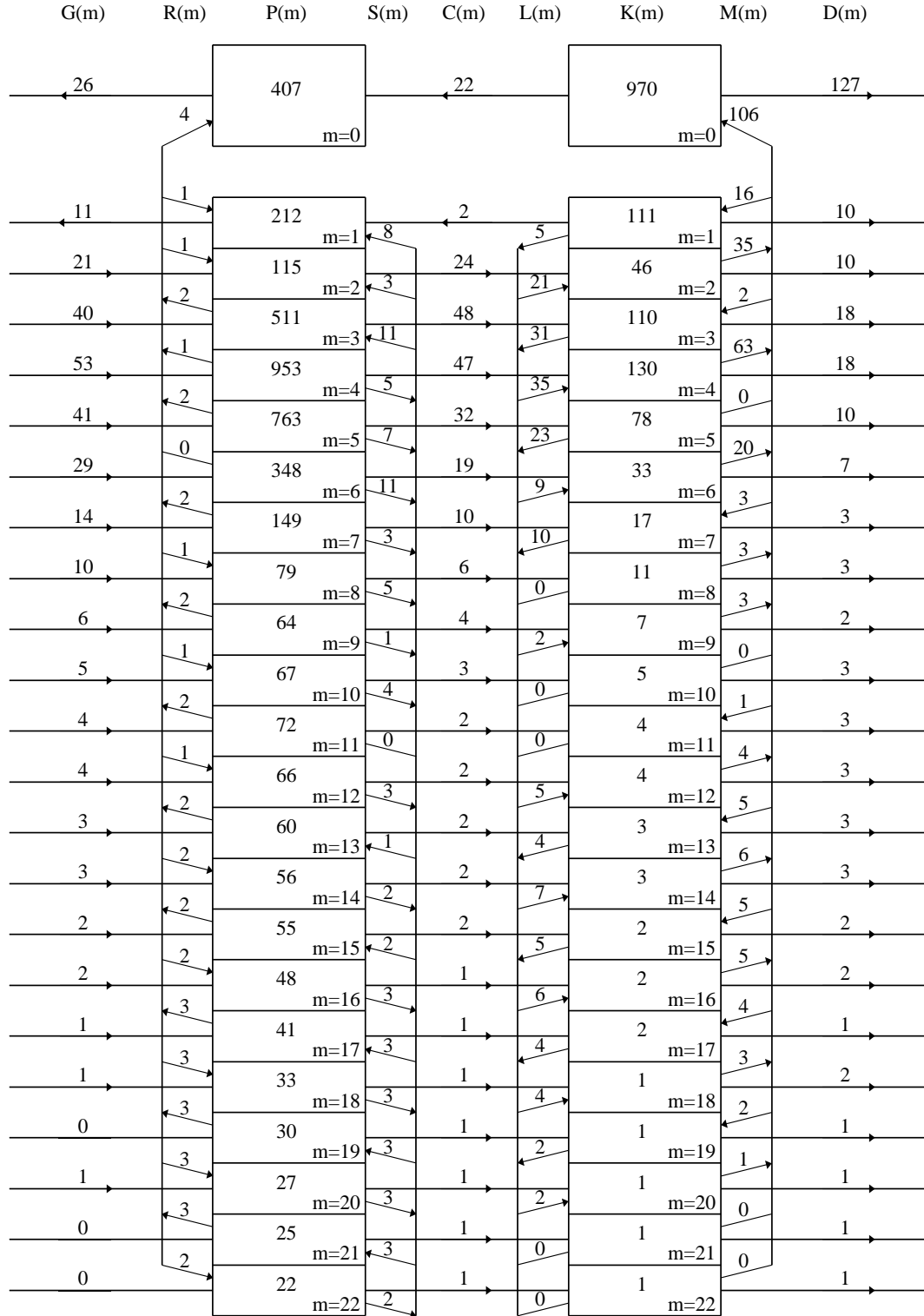


Figure 4.2. The energy flow diagram of the atmospheric general circulation in the vertical spectral domain. The data used in this figure are the entire period of JRA-25 and JCDAS. The units of the energy are 10^3J/m^2 , and those of the interactions term are 10^{-2}W/m^2 .

4.1.2 Seasonal mean energetics

The seasonal differences of the energy spectrum and energy interactions are also analyzed. The energetics terms of the barotropic and baroclinic components are listed in Table 4.1 at each season in Northern and Southern Hemispheres. The baroclinic available potential energy P_s is very large and similar amount of energy in the winter hemisphere, whose amount is $4.884 \times 10^6 \text{ J/m}^2$ and $4.769 \times 10^6 \text{ J/m}^2$ in Northern and Southern Hemispheres, respectively. In summer hemisphere, the baroclinic available potential energy have minimum value compared to every season. The value of the baroclinic conversion in winter hemisphere has also largest value in all seasons. The barotropic-baroclinic interactions of kinetic energy have similar values in Northern Hemisphere through the year. However in Southern Hemisphere, they differ by seasons and the those in winter have a very small value, 0.52 W/m^2 .

The magnitude of the kinetic energy is influenced by the strength of the jet stream. The kinetic energy in the Southern Hemisphere becomes larger than that in the Northern Hemisphere, because of the difference of the strength of the jet stream due to the topography. The jet stream becomes strong in the winter hemisphere, and weak in the summer hemisphere. The barotropic kinetic energy in DJF in Northern Hemisphere ($1.217 \times 10^6 \text{ J/m}^2$) is about three times large as the baroclinic kinetic energy ($0.386 \times 10^6 \text{ J/m}^2$). The ratios of the barotropic and baroclinic kinetic energies (K_s/K_M) are about 0.70 and 0.50 in the Northern and Southern Hemispheres, respectively, except the summer hemisphere. In summer hemisphere, the ratio be-

comes larger, which means that the baroclinicity becomes stronger. Especially in the summer in the Northern Hemisphere, the ratio reaches 1.03, the baroclinic kinetic energy becomes stronger than the barotropic kinetic energy.

Figures 4.3 (a)-(d) show the same category of Fig. 4.1, but for the December, January and February (DJF), March, April and May (MAM), June, July and August (JJA), and September, October and November (SON), respectively. The available potential energies for $m = 4$ in MAM and DJF are $1.051 \times 10^6 \text{ J/m}^2$ and $1.219 \times 10^6 \text{ J/m}^2$, respectively. On the other hand, the available potential energies for $m = 4$ in JJA and SON are $0.61 \times 10^6 \text{ J/m}^2$ and $0.857 \times 10^6 \text{ J/m}^2$, respectively. The interactions of the available potential energy and the baroclinic conversion have almost the same values in every season. The baroclinic-baroclinic interactions of the kinetic energy vary with the seasons, especially in the lower order vertical modes. The kinetic energy for $m = 4$ receives the kinetic energy from baroclinic-baroclinic interactions, and gives it to the barotropic mode, in every season. This is caused by the barotropization of the tropospheric jet induced by the baroclinic instability. The kinetic energy for $m = 2$ also receives it from baroclinic-baroclinic interactions, and gives it to the barotropic mode except for DJF, despite of having a local minimum kinetic energy.

Table 4.1. The ratio of barotropic and baroclinic kinetic energy. The units of energy are 10^5 J/m^2 .

	season	P_M	P_s	K_M	K_s	K_s/K_M	C_s	$M(0)$	D_s	D_M
Northern Hemisphere	DJF	4.26	48.84	12.17	7.58	0.62	2.61	1.05	1.33	0.90
	MAM	2.38	37.62	7.87	5.65	0.72	1.89	1.15	1.03	0.96
	JJA	1.48	23.29	3.86	3.98	1.03	1.58	0.96	1.05	0.79
	SON	2.54	31.87	7.13	4.56	0.64	1.97	1.17	0.99	1.00
	Annual	2.66	35.35	7.74	5.44	0.70	2.01	1.08	1.10	0.91
Southern Hemisphere	DJF	2.69	33.66	7.33	5.14	0.70	1.54	1.42	0.82	1.26
	MAM	4.69	38.37	10.44	5.03	0.48	2.10	0.90	1.07	0.68
	JJA	8.19	47.69	15.35	7.10	0.46	2.63	0.52	1.25	0.15
	SON	5.69	40.51	11.93	6.40	0.53	2.03	1.18	0.99	0.92
	Annual	5.39	40.09	11.28	5.92	0.52	2.08	1.00	1.03	0.75

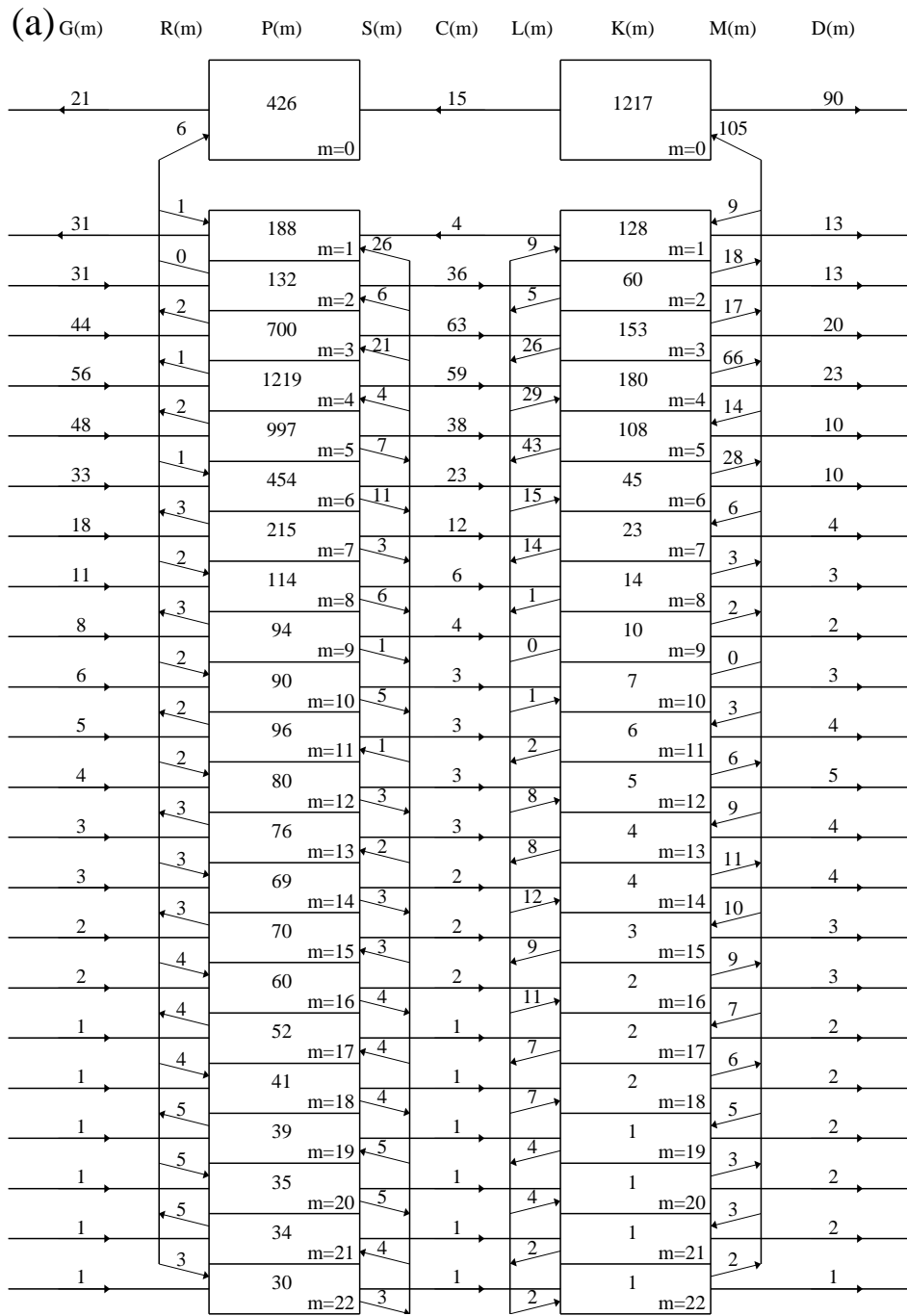


Figure 4.3. As in Fig. 4.2 except for (a) DJF, (b) MAM, (c) JJA, (d) SON.

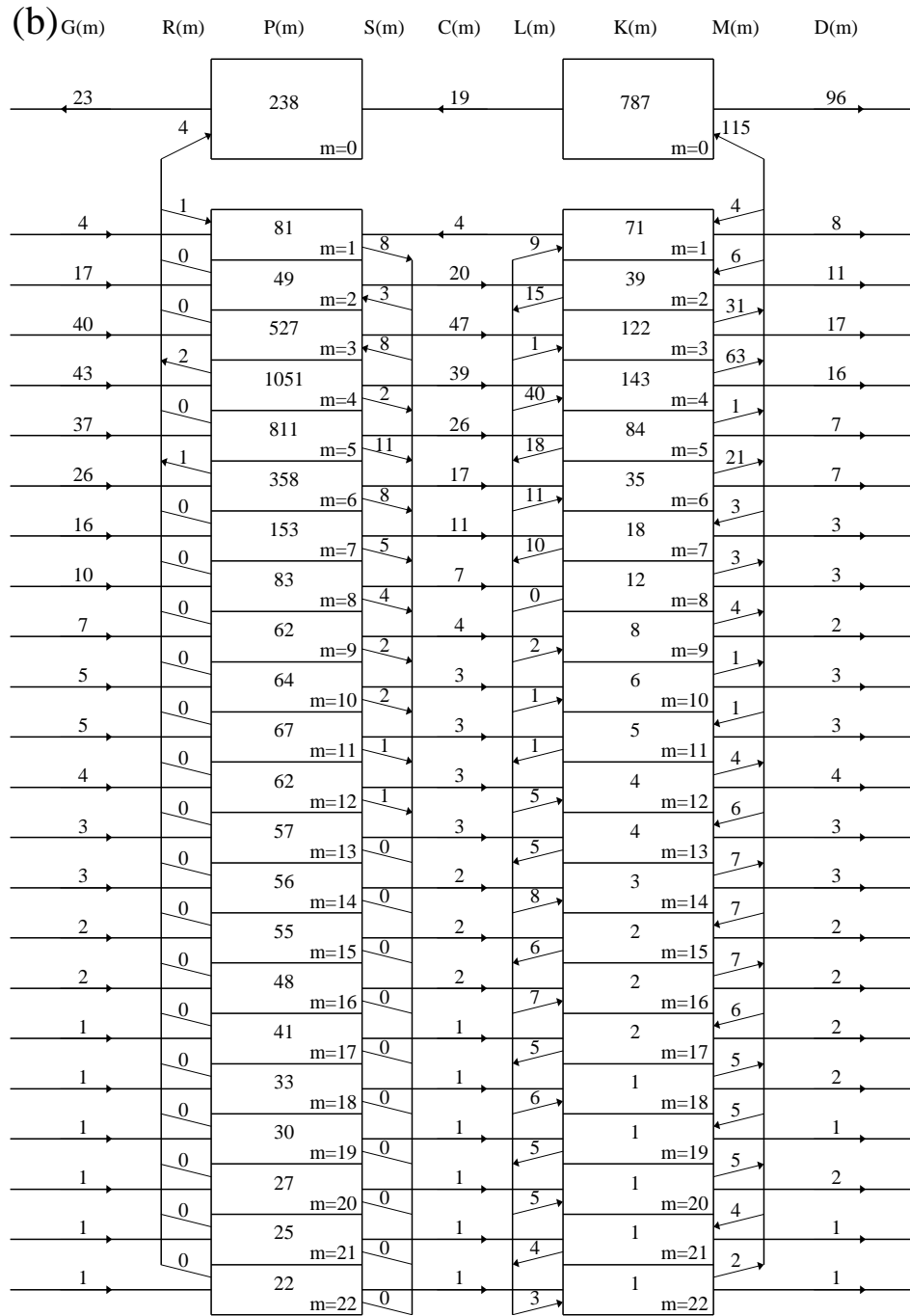


Figure 4.3. Continued.

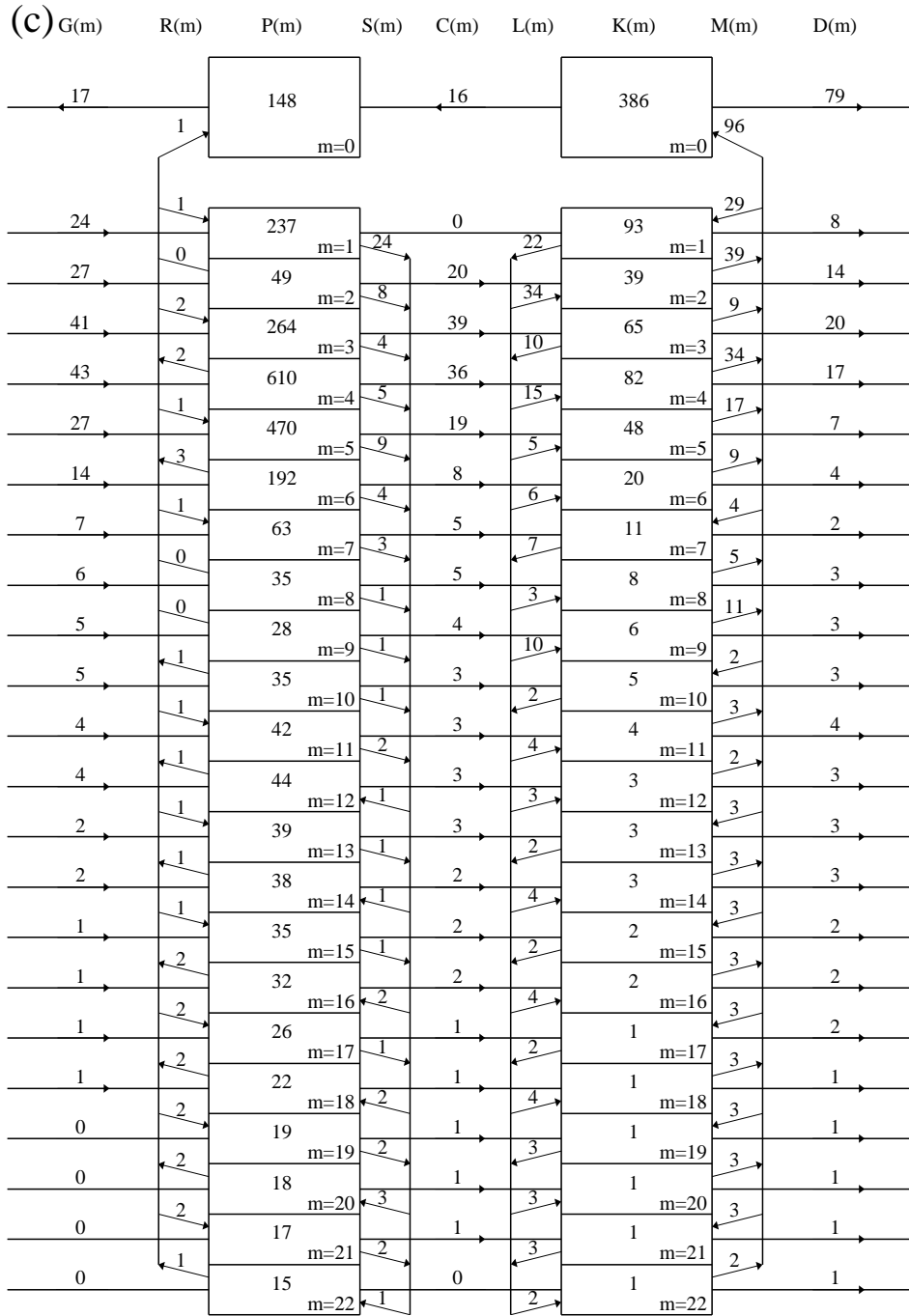


Figure 4.3. Continued.

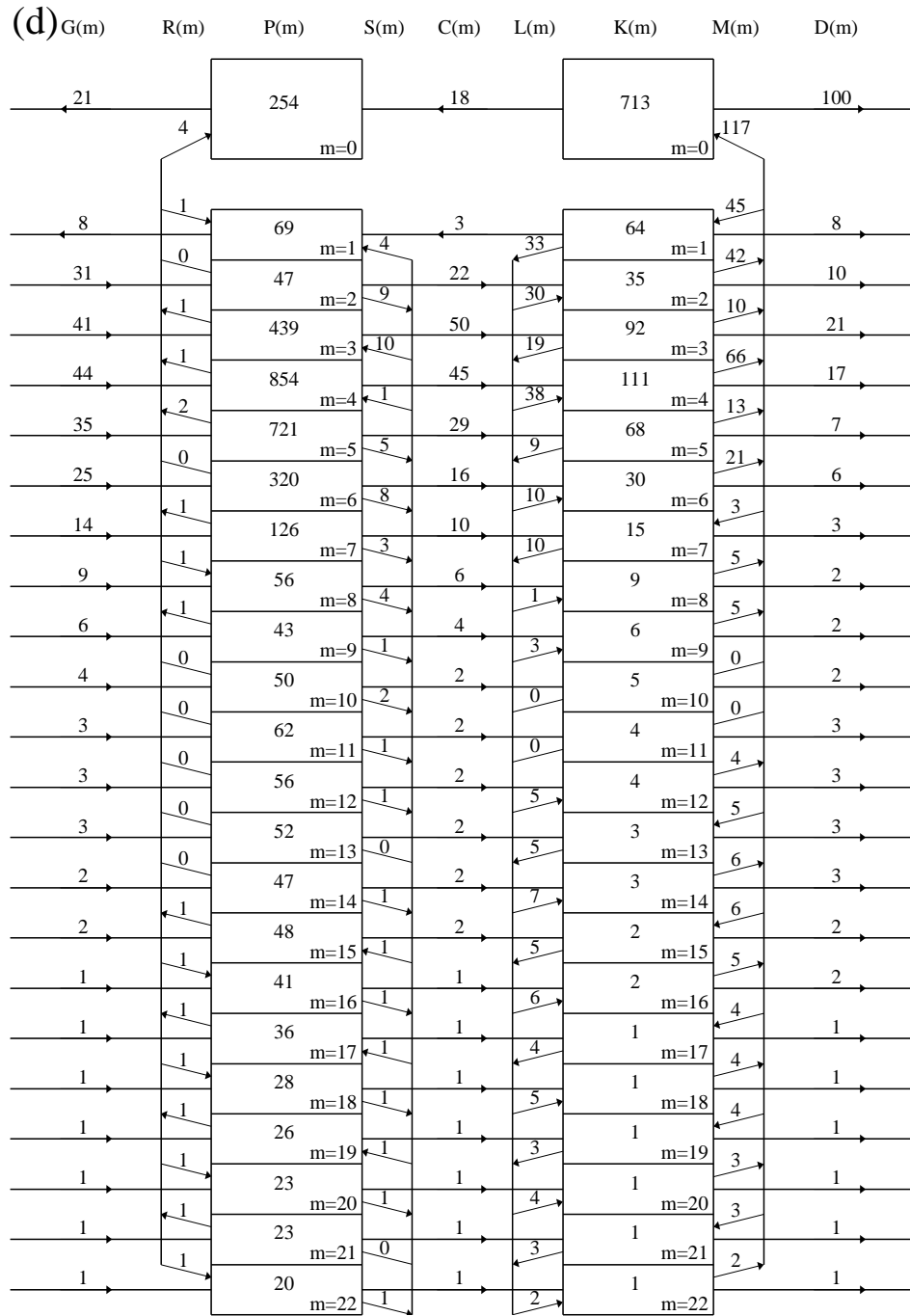


Figure 4.3. Continued.

4.1.3 Horizontal distribution

Kinetic energy of the atmosphere is mostly included in the tropospheric jet region. Chen and Yen (1983) pointed out that a three-jet structure emerges in the winter circulation in the Northern Hemisphere. These jets appear over the east coast of both Asia and North America, and over North Africa.

Figure 4.4 shows the kinetic energy distributions of the barotropic and baroclinic components in the Northern Hemisphere. The atmospheric energy is mostly included in the mid-latitude jet region. The energy peak of the baroclinic mode is located somewhat in the west of the barotropic peak. The amount of the energy peak of the three jet regions are listed in the Table 4.2. The Asian jet is the strongest in these three jets, and the amounts of the barotropic and baroclinic modes are 6.2×10^6 J/m² and 3.1×10^6 J/m², respectively. The other two jets over North America and North Africa are weaker than the jet over Asia. The amounts of barotropic energy over American and African jets are 3.9×10^6 J/m² and 2.8×10^6 J/m², respectively. The ratios of the barotropic kinetic energy of the North African jet and Asian jet for the total energy are 62% and 67%, respectively. On the other hand, the ratio of the barotropic kinetic energy of the North American jet for the total energy reaches 80%. According to this analysis, it is found that the North American jet has the strongest barotropy in these three jets.

Figure 4.5 shows the kinetic energy distributions of baroclinic modes from $m = 1$ to $m = 8$. The vertical mode $m = 1$ has a specific distribution, which is an energy

peak around the polar region. This distribution corresponds to the polar vortex in the stratosphere. The energy of the Asian jet of the baroclinic mode is mostly included in vertical mode $m = 4$, and the maximum value of the Asian jet is $9 \times 10^5 \text{ J/m}^2$. The baroclinic energy of the Asian jet is distributed around vertical mode $m = 4$, the energy for $m = 1$, $m = 3$, and $m = 5$ is $4 \times 10^5 \text{ J/m}^2$, $8 \times 10^5 \text{ J/m}^2$, and $5 \times 10^5 \text{ J/m}^2$, respectively. About 85% of the Asian jet energy for baroclinic mode can be explained by the vertical modes $m = 1, 3, 4$, and 5 .

Figure 4.6 illustrates the horizontal distributions of the kinetic energy generations for barotropic and baroclinic modes in the Northern Hemisphere. As is mentioned above, the integral of the kinetic energy generation of the barotropic mode over the Northern Hemisphere is insignificant. Therefore, the baroclinic kinetic energy generation is essentially responsible for the maintenance of atmospheric kinetic energy in the Northern Hemisphere. But the local barotropic kinetic energy generation has a considerable value. The positive kinetic energy generations are found in the upstream side of jet from the east Asia to Japan, and negative values are found in the downstream side of jet around the central Pacific ocean. There is no significant kinetic energy generation in the African jet region, however there are clear kinetic energy peaks in both barotropic and baroclinic modes. The generation over the east coast of America is also found. However, the amount is about half less than over the east coast of Asia. The kinetic energy generation over the Tibetan plateau has a complex distribution because of a complex topography.

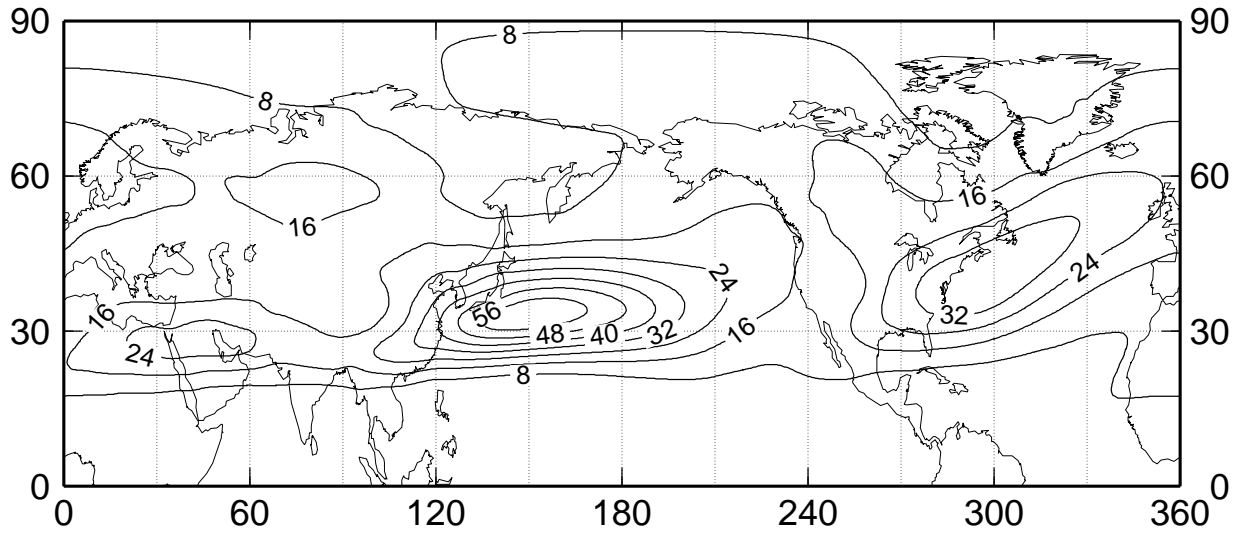
The kinetic energy converted from available potential energy in the baroclinic

atmosphere is transformed to kinetic energy of the barotropic mode. Figure 4.8 shows the horizontal distribution of the barotropic-baroclinic interactions of kinetic energy in the Northern Hemisphere. The locations of the peak of the barotropic-baroclinic interactions of kinetic energy correspond to the locations of the barotropic kinetic energy peak, except for the African jet. The peak of the barotropic-baroclinic interactions of kinetic energy in Asian jet is located somewhat east of the peak of the baroclinic kinetic generation. Another peak of the barotropic-baroclinic interactions exists in the upstream side of the Rocky Mountain. There is an interesting distribution in the Greenland. The negative region broadens over the land of Greenland, and the positive value distributes over the coast in the south of Greenland.

Table 4.2. The energy of the 3 jet resions. The units of energy are 10^6 J/m².

	barotropic	baroclinic	total
Africa	2.8 (62%)	1.7 (38%)	4.5
Asia	6.2 (67%)	3.1 (33%)	9.3
America	3.9 (80%)	1.3 (20%)	4.9

Barotropic Kinetic Energy



Baroclinic Kinetic Energy

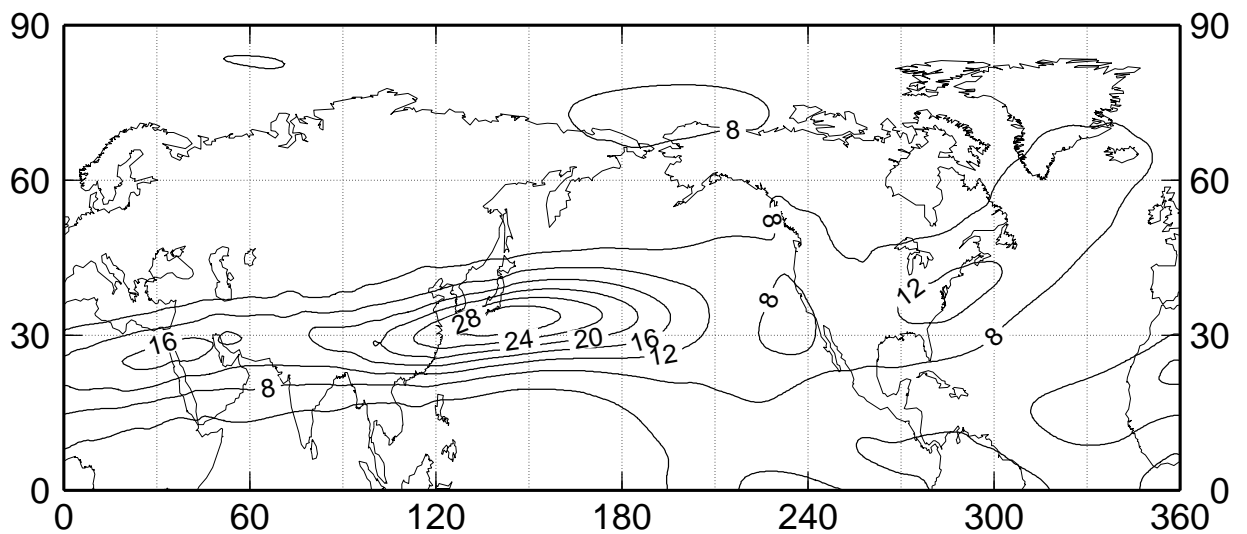


Figure 4.4. The horizontal distributions of barotropic (upper) and baroclinic (bottom) kinetic energies for Northern Hemisphere. The Units of energy are 10^5 J/m^2 . The contour interval for barotropic mode is $8 \times 10^5 \text{ J/m}^2$ and for baroclinic mode is $4 \times 10^5 \text{ J/m}^2$.

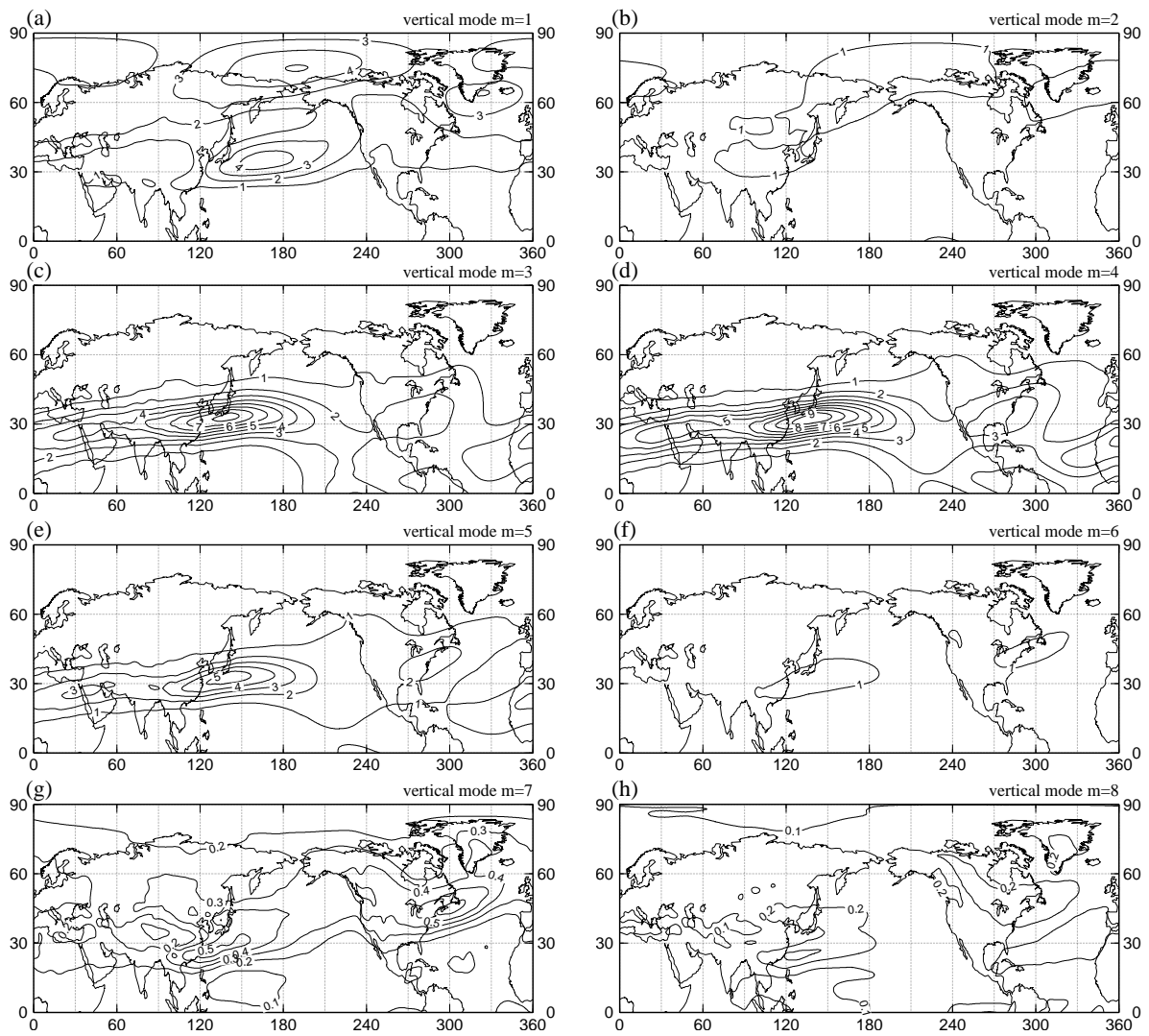
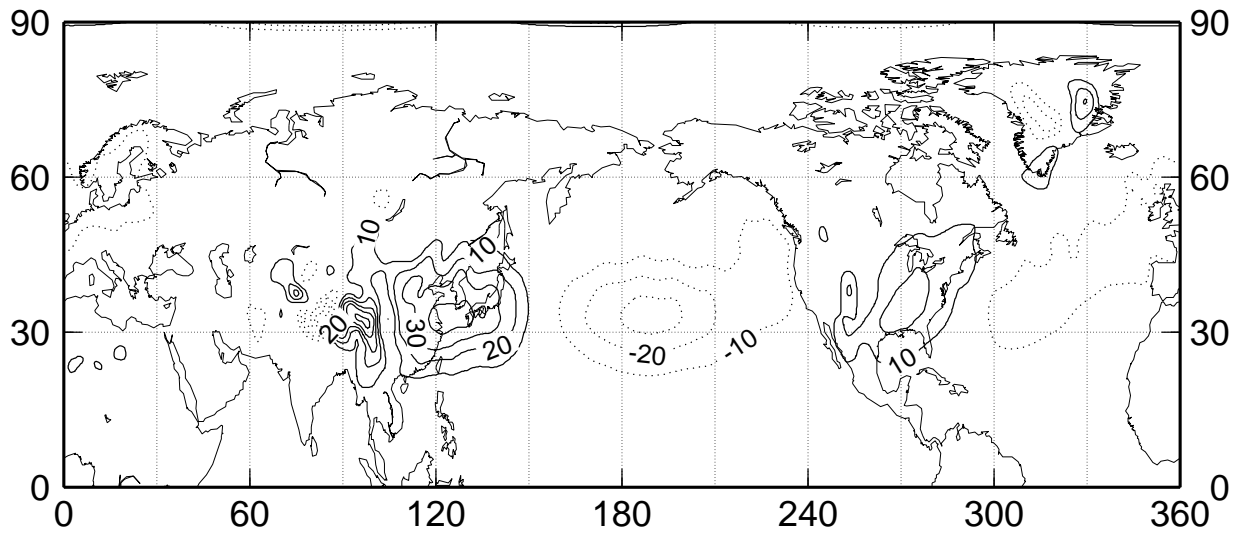


Figure 4.5. The horizontal distributions of kinetic energy for vertical mode $m = 1$ to 8. The units of energy are 10^5 J/m^2 . The contour intervals for $m = 1$ to 6 are $1 \times 10^5 \text{ J/m}^2$ and for $m = 7$ and 8 are $0.5 \times 10^5 \text{ J/m}^2$.

Barotropic Kinetic Energy Generation



Baroclinic Kinetic Energy Generation

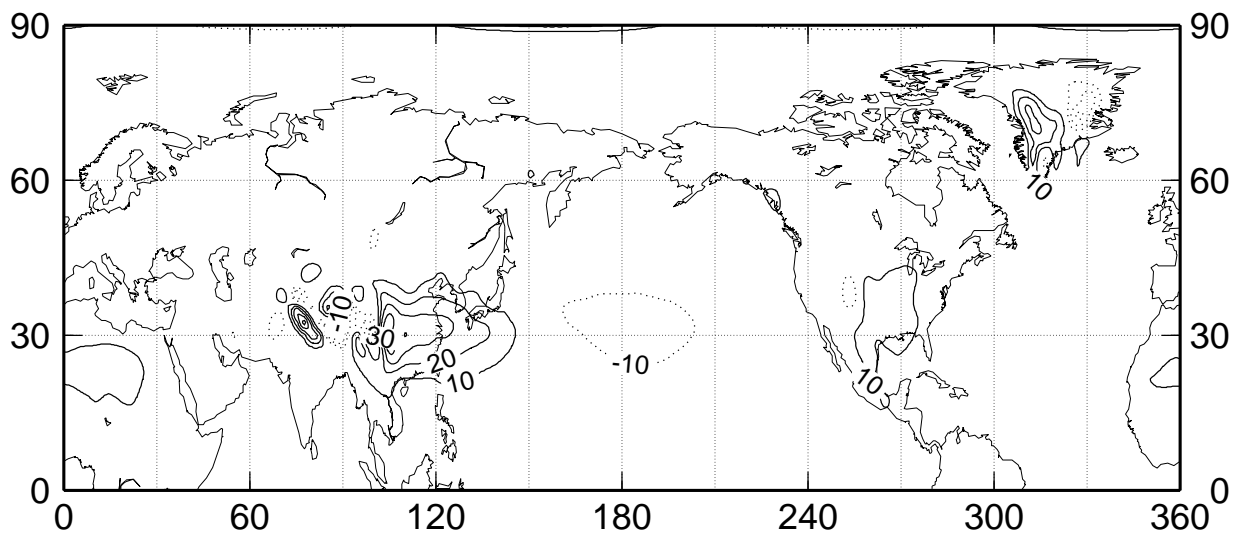


Figure 4.6. The horizontal distributions of the kinetic energy generations for barotropic (upper) and baroclinic (bottom) modes in the Northern Hemisphere. The units are W/m^2 . Contour interval is $10 \text{ W}/\text{m}^2$.

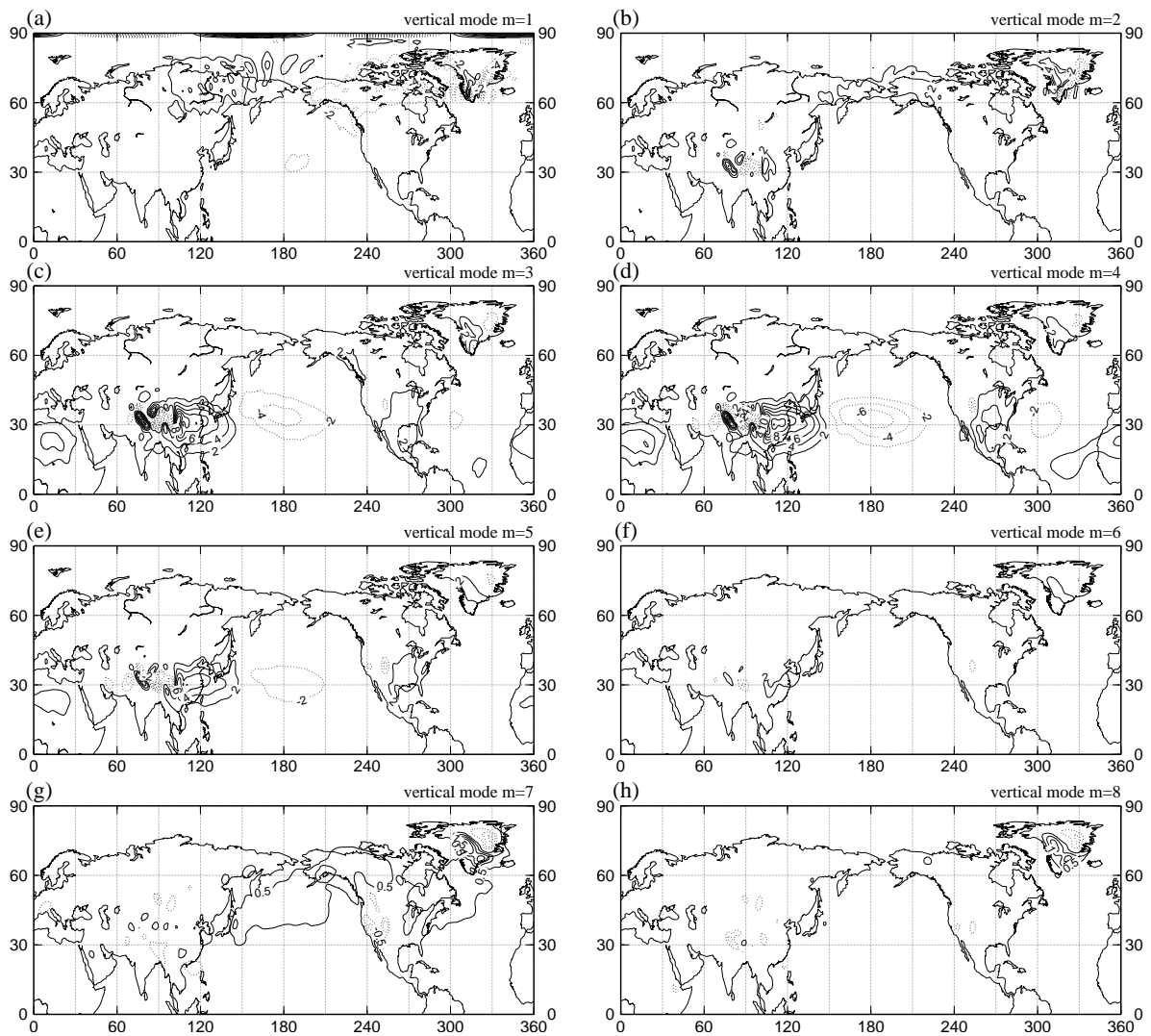


Figure 4.7. The horizontal distributions of kinetic energy generation for vertical mode $m = 1$ to 8. The units of energy generation are W/m^2 . The contour intervals for $m = 1$ to 6 are $2 \text{ W}/\text{m}^2$ and for $m = 7$ and 8 are $0.5 \text{ W}/\text{m}^2$.

Barotropic-Baroclinic Interactions of Kinetic Energy

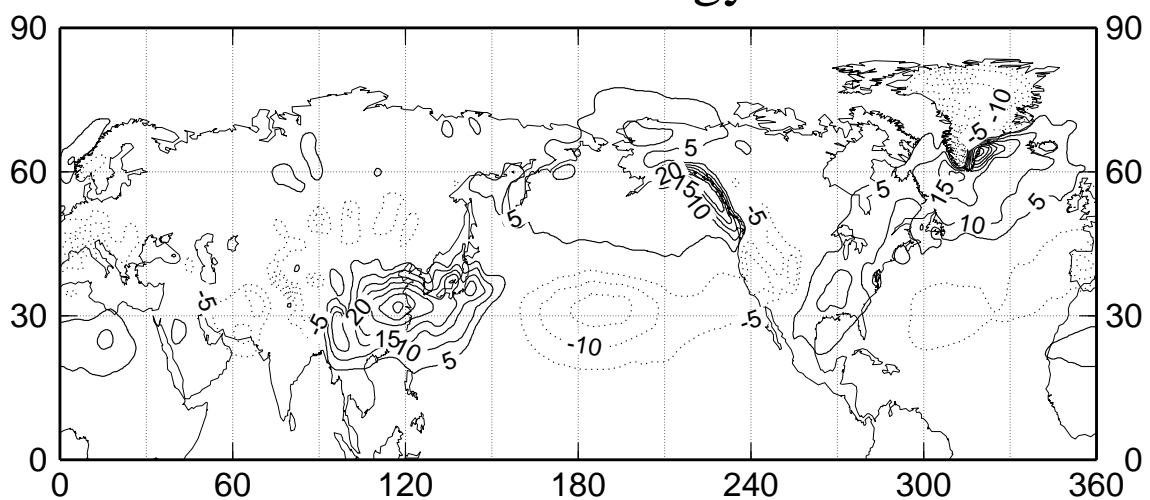


Figure 4.8. The horizontal distributions of the barotropic-baroclinic interactions of kinetic energy in the Northern Hemisphere. The units are W/m^2 . Contour interval is $5 \text{ W}/\text{m}^2$.

4.1.4 Difference in the vertical energy spectrum using numerical and analytical vertical structure functions

Tanaka (1985) investigated energetics of the atmospheric general circulation expanded with 3D normal mode functions, which includes the numerical vertical structure functions. The numerical vertical structure functions have a large aliasing in the higher order vertical modes (Fig. 2.1b). Figure 4.9 shows the total energy spectrum in the vertical wavenumber domain expanded by the numerical vertical structure functions, where the total energy is the summation of the kinetic energy and available potential energy. Although the sum of the total energy represents the global integral for the total energy over the sphere, the spectrum is highly irregular indicating three peaks at barotropic mode, 2.147 ($m=8$), and 23.908 (higher order modes), respectively. A notable energy gap is seen at 3.413 ($m=12$) which may corresponds to the Nyquist wavenumber.

In contrast, Fig. (4.10) shows the kinetic and available potential energy spectra expanded by the analytical vertical structure functions for JRA-25. The vertical energy spectrum is basically red spectrum in that the total energy is high in lower order modes and low in higher order modes. There is a marked energy peak at the vertical wavenumber 1.8266 ($m=4$) for both kinetic energy and available potential energy. The half vertical wavelength of the vertical mode $m=4$ is about 13.7 km, which is corresponds to the scale of the thickness of the troposphere. This energy peak is caused by the vertical structure function for $m=4$ having a maximum at about 200 hPa and the opposite sign at low troposphere, as seen in Fig. 2.2(a).

The tropospheric jet around upper troposphere may cause the secondary maximum of kinetic energy. The baroclinic structure of geopotential deviation from the global mean, which has an opposite sign at low and high troposphere, may be reflected at $m=4$. The total energy at this peak is mostly explained by the available potential energy, whereas the barotropic energy is mostly contained in kinetic energy. The kinetic energy spectrum has an interesting slope in the higher wavenumber than the scale of the second energy peak. It is found in this study that the kinetic energy obeys -3 power of the non-dimensional vertical wavenumber μ_m in common with the -3 power law in the horizontal wavenumber domain.

The result obtained in this study shows significant contrast with the vertical energy spectrum by Tanaka (1985) and Tanaka and Kung (1988), where the spectrum in the higher order vertical modes appears to be zigzag as in Fig. 4.9 by the influence of aliasing due to the numerical solutions.

Vertical Energy Spectrum

1 Jan 1979 - 31 Jan 1979

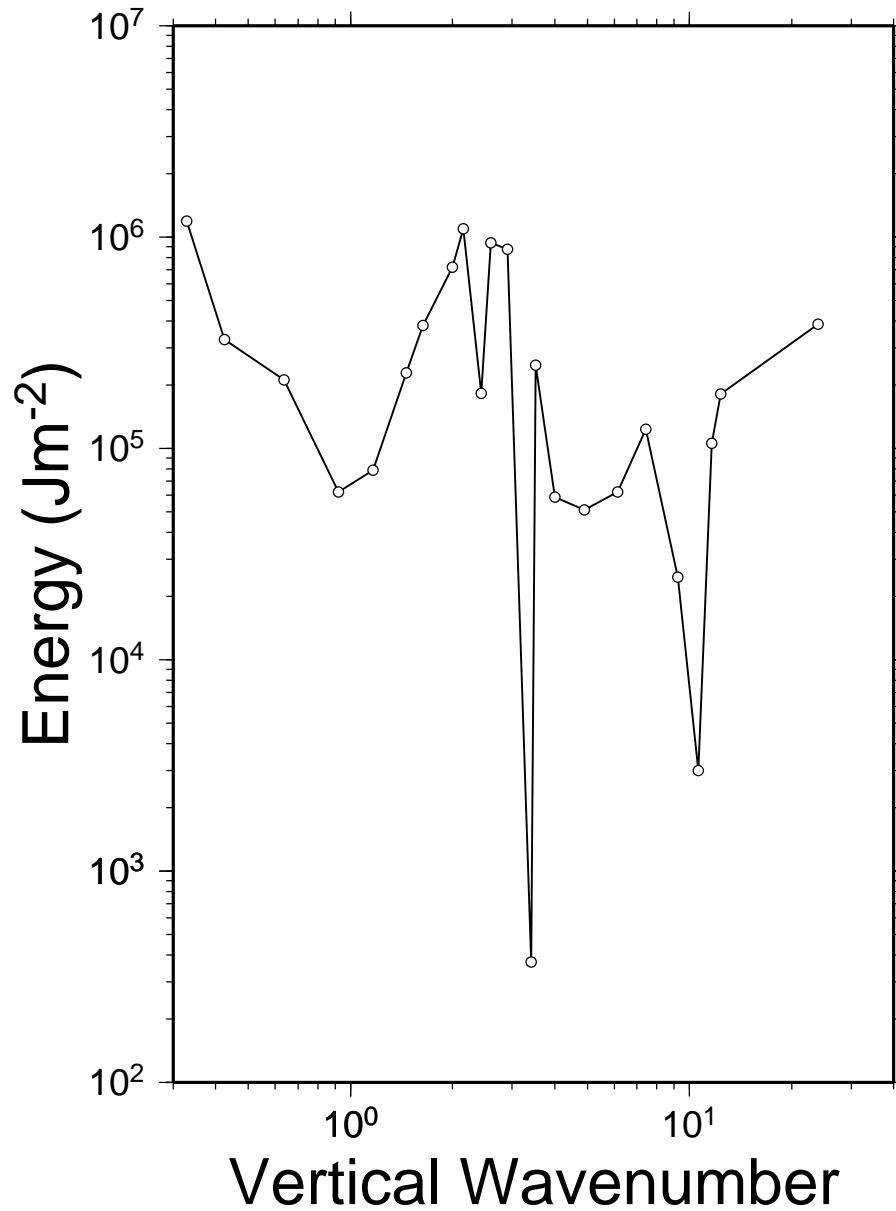


Figure 4.9. The vertical energy spectrum expanded by the numerical vertical structure functions. The data period are from 1 Jan 1979 to 31 Jan 1979. The units of energy are J/m^2 .

Vertical Energy Spectrum

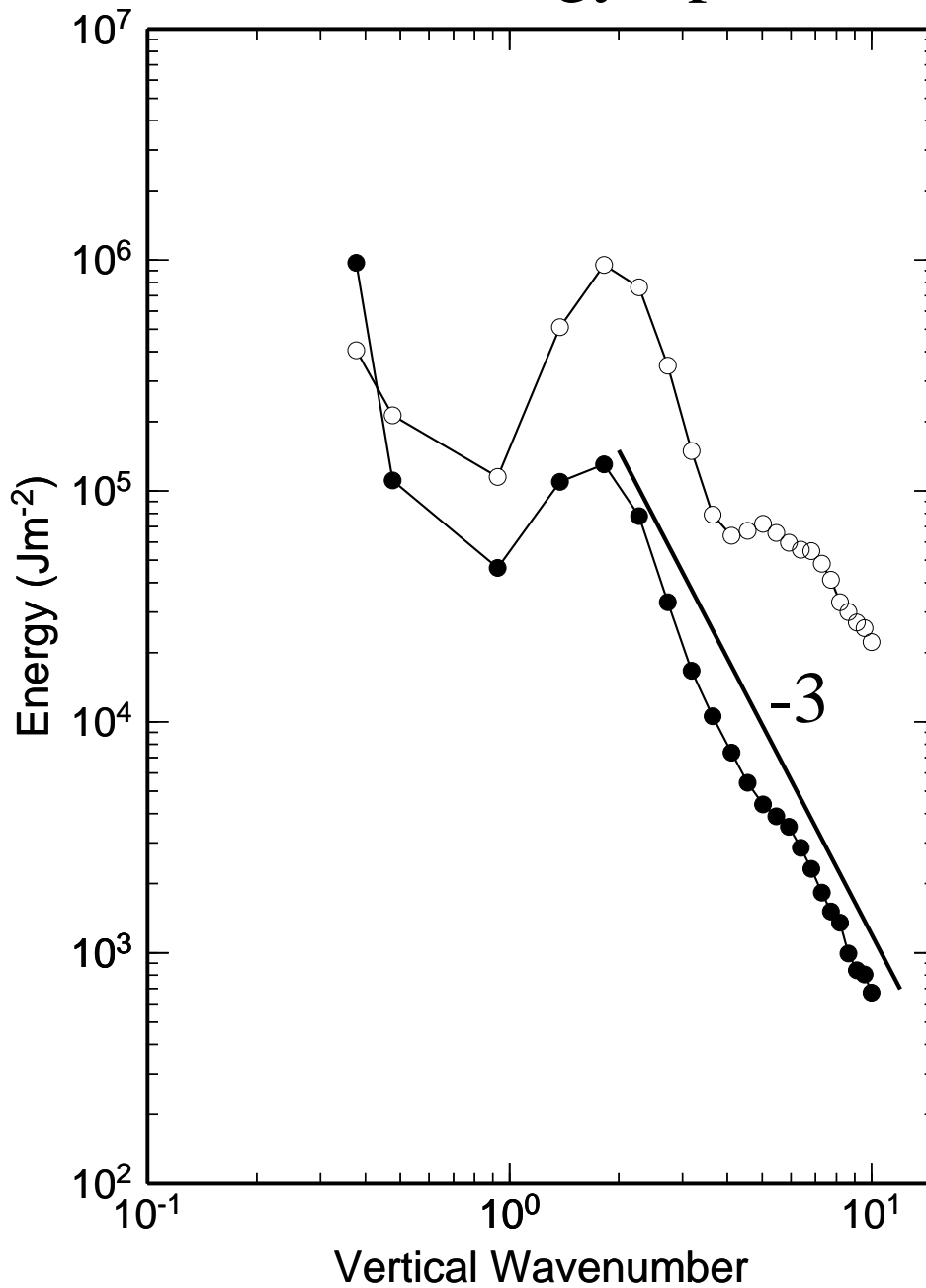


Figure 4.10. Energy spectra of kinetic and available potential energies expanded by the analytical vertical structure functions. The data period are from 1979 to 2007. The units of energy are J/m².

4.2 3D Normal Mode Energetics

4.2.1 Energy spectrum of the barotropic atmosphere

Tanaka et al. (2004) investigated the characteristic of the energy spectrum for barotropic motion in the phase speed domain. The spectral characteristic for the barotropic component in the phase speed domain was argued by Tanaka et al. (2004), by using a criterion, which is a Rossby wave breaks down when a local meridional gradient of the potential vorticity is negative, i.e., $\partial q/\partial y < 0$, somewhere in the domain. Using this criterion, they derived that the energy spectrum is proportional to c^2 (Fig. 4.11) and also the barotropic energy spectrum of the general circulation E can be represented as:

$$E = mc^2, \quad (4.1)$$

where m is the total mass of the atmosphere for unit area.

Figure 4.11 illustrates the barotropic energy spectrum E_i and the energy flux F_{Wi} in the phase speed domain (see Terasaki and Tanaka 2007). The energy levels are connected by the dotted line for the same zonal wavenumber n with different meridional mode number l . The red line in the figure denotes the spectral slope of $E = mc^2$ derived by Tanaka et al. (2004) from the criterion of the Rossby wave saturation, $\partial q/\partial y < 0$ (Garcia, 1991). The energy spectrum indicates the two different regimes with distinct slopes for small c_i and large c_i . According to this figure, it is found that the energy spectrum obeys approximately the 2 power law of the phase speed of

Rossby wave for small c_i in the turbulent regime $R_i > 1$.

The atmospheric energy is converted from the baroclinic to the barotropic components at the synoptic scale motions when the baroclinicity is removed by the baroclinic instability. The energy injected at the synoptic scale ($c_i=0.004$) cascades up to the larger scale obeying the 2 power law of the phase speed c_i (Tanaka et al. 2004). The up-scale energy cascade is, however, arrested at the Rhines scale C_R , beyond which the linear term dominates ($R_i < 1$), due to the increased σ or c . The energy spectrum is much steeper than the c^2 in the short wave range where the energy cascades down.

The characteristic spectral slope in the barotropic atmosphere can be obtained from eq.(4.1) by applying the dispersion relation of Rossby wave. The phase speed of the Rossby wave is given by a total wavenumber k on the β plane,

$$c = -\frac{\beta}{k^2}. \quad (4.2)$$

If we substitute this relation into Eq. (4.1), we obtain the following relation,

$$E(k) = m\beta^2 k^{-4}. \quad (4.3)$$

If we assume the isotropy for zonal wind u and the meridional wind v over the range of synoptic to short waves, the energy spectrum can be expressed as a function of zonal wavenumber n instead of total wavenumber k .

$$E(n) \simeq m\beta^2 n^{-4}. \quad (4.4)$$

According to Eq. (4.4), it is inferred that the energy spectrum in the zonal wavenumber domain obeys -4 power of the zonal wavenumber.

Figure 4.12 illustrates the zonal energy spectrum of Rossby mode and gravity mode for the barotropic component. The red line in the figure denotes the spectral slope of the -4 power of the zonal wavenumber inferred by the theory. According to the result, it is found that the observed zonal energy spectrum exactly obeys the -4 power of the zonal wavenumber for synoptic scale motions ($n = 9 - 30$). The zonal energy spectrum for planetary scale is less steeper than that for synoptic scale, and that beyond $n = 35$ is much steeper than the -4 power law.

The energy level of the gravity mode for barotropic component is very small compared to the Rossby mode. The eddy energy peak exists in the zonal wavenumber $n = 2$. The spectral slope is apparently different from that of the Rossby wave saturation theory in this range.

Figure 4.13 illustrates the zonal energy spectrum of Rossby mode and gravity mode as in Fig. 4.12, but for the baroclinic component. The red and blue lines in the figure denote the spectral slope of the -3 and -4 powers of the zonal wavenumber. According to the result, it is confirmed that the observed zonal energy spectrum approximately obeys the -3 power of the zonal wavenumber for synoptic scale motions as is consistent with previous numerous studies. Hence, the characteristic -4 power law is specific only to the barotropic component of the atmosphere.

In Figs. 4.12 and 4.13, the energy slopes for the higher wavenumber of the Rossby mode do not obey the specific laws, but they become steeper.

Total Energy Spectrum

DJF Climate (1979 - 2000)

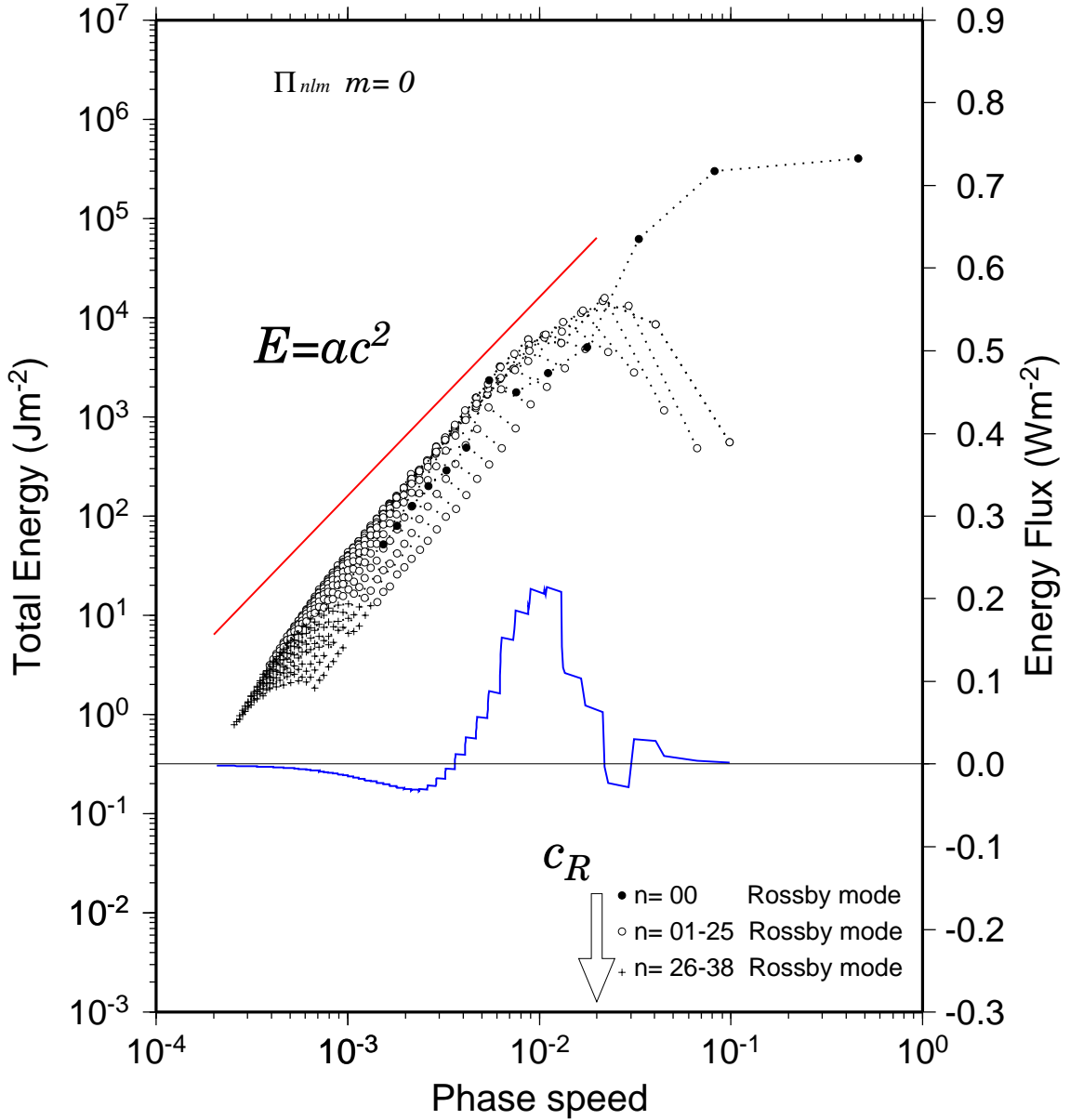


Figure 4.11. The total energy spectrum E_i and the energy flux associated with the nonlinear wave-wave interactions for the barotropic component in the dimensionless phase speed of the Rossby mode c_i evaluated for the 22 years of the JRA-25 during the winter DJF. Energy levels are connected by the dotted lines for the same zonal wavenumber n with the different meridional mode numbers l . The red line of the $E = ac^2$ represents the energy slope derived from the condition of the Rossby wave breaking, $\partial q / \partial y < 0$.

Zonal Energy Spectrum

DJF Climate (1979 - 2000)

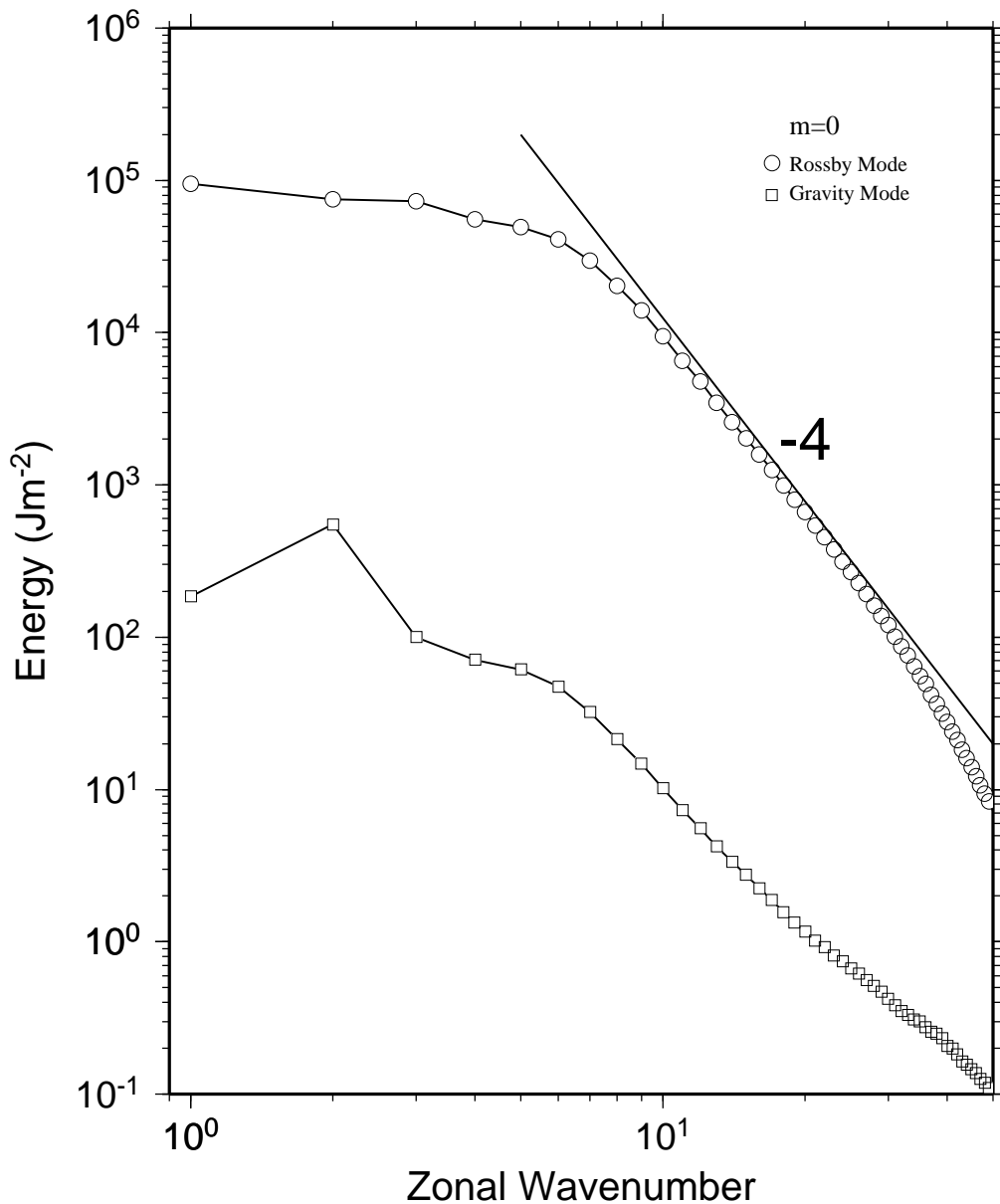


Figure 4.12. The eddy energy spectrum of the Rossby and gravity modes for the barotropic component as a function of the zonal wavenumber evaluated for the 22 years of the JRA-25 during the winter DJF. Circles and square denote the energy for Rossby and gravity modes, respectively. The solid line in the figure denotes the spectral slope of -4 power derived from Eq. (4.4).

Zonal Energy Spectrum

DJF Climate (1979 - 2000)

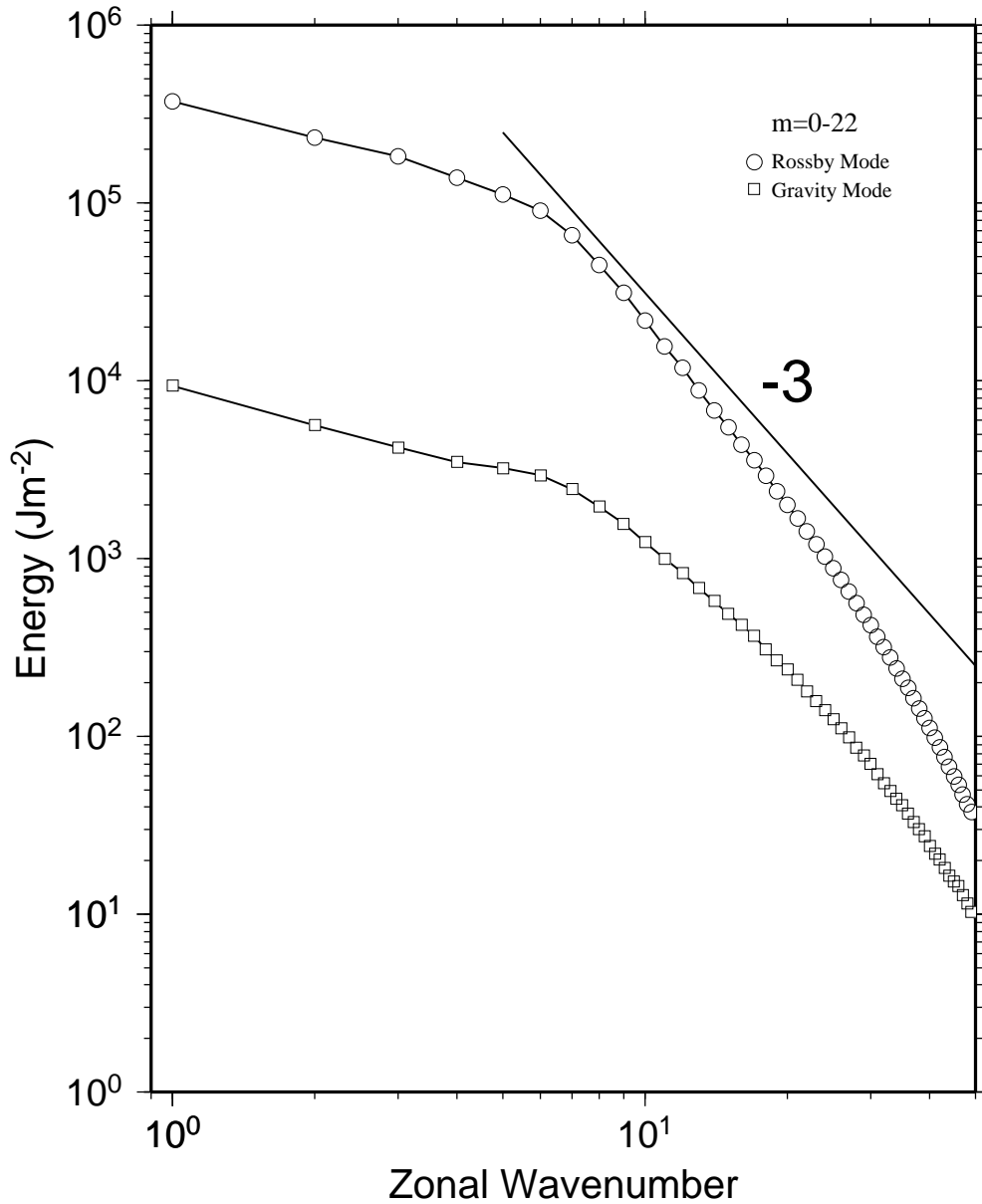


Figure 4.13. As in Fig. 4.12, but for the sum of the barotropic and baroclinic components of the atmosphere. The solid lines in the figure denotes the spectral slope of -3 power.

4.2.2 Energy interactions

Energy interactions in the zonal wavenumber domain and in the vertical spectral domain are analyzed in this subsection based on (2.48). Figure 4.14 illustrates the nonlinear interactions of kinetic energy and available potential energy in the zonal wavenumber domain ($n = 1 - 25$) by (a) summing all vertical modes ($m = 0 - 22$), (b) for the barotropic mode ($m = 0$), and (c) for the baroclinic modes ($m = 1 - 22$), respectively. Similarly, Fig. 4.15 illustrates the nonlinear interactions in the vertical mode domain ($m = 0 - 22$) by (a) summing all zonal wavenumbers ($n = 0 - 50$), (b) for zonal component ($n = 0$), and (c) for all eddy components ($n = 1 - 50$). Those energy interactions are supposed to vanish when summed over the all wavenumbers due to the energy conservation law. However, the summation of the available potential energy interactions, term C , did not vanish by some assumptions involved and the accumulation of computational error. We thus have adjusted the errors at the zonal component by redistributing it linearly as a function of the vertical and meridional wavenumbers to meet the conservation law. Such an adjustment was not necessary for the term B .

According to the result of the analysis, energy of the general circulation of the atmosphere is first supplied at the available potential energy of zonal baroclinic components by the differential heating of the solar radiation, as indicated by negative values of C in Fig. 4.15 (b). The negative values are balanced by positive values of the interactions C at eddy baroclinic components as seen in Fig. 4.15 (c) and in Fig. 4.14

(c). This means that the zonal available potential energy is transformed into the eddy available potential energy, both of which are contained in the baroclinic component of the atmosphere. As seen in Fig. 4.14 (c), the eddy available potential energy is converted into the eddy kinetic energy as seen by the opposite signs of B and C . It is also found that the baroclinic eddy kinetic energy is transformed into barotropic kinetic energy as seen by positive B in Fig. 4.14 (b) and in Fig. 4.15 (c). The eddy barotropic energy accumulated at synoptic to planetary waves is finally transformed to zonal barotropic energy as seen by positive B in Fig. 4.15 (b). The kinetic energy supplied to barotropic mode is dissipated by surface friction and viscosity. These results are consistent with Tanaka and Kung (1988), which have been analyzed using the numerical vertical structure functions.

The effect of using the analytical vertical structure functions is found at the nonlinear interactions for the higher order vertical modes. Small but consistently negative values of the available potential energy interactions over $m > 6$ in Fig. 4.15 (b) indicate that an energy source of the atmospheric general circulation exists in higher order vertical modes. There are some available potential energy source at $m = 1$ and 3. The kinetic energy interactions are hardly seen in the higher order vertical modes (Figs. 4.15b and c).

Figure 4.16 shows the energy flux of kinetic energy (F_B), available potential energy (F_C), and total energy (F_N) in the vertical wavenumber domain. Negative and positive values indicate upscale and downscale cascades, respectively. It is shown that energy flux basically shows negative value, indicating dominant inverse energy

cascade from smaller vertical scale to larger vertical scale motions. As a result, the atmospheric energy is transformed from baroclinic to barotropic components. The kinetic energy flux is the largest at the vertical wavenumber 0.00125 ($m=2$), and peak of the available potential energy flux is seen at 0.01186 ($m=7$). It is suggested from these analyses using the analytical vertical structure functions that the energy interactions are performed by relatively larger vertical scale motions for the kinetic energy, whereas there is a complex structure of the available potential energy interactions in the higher order vertical modes.

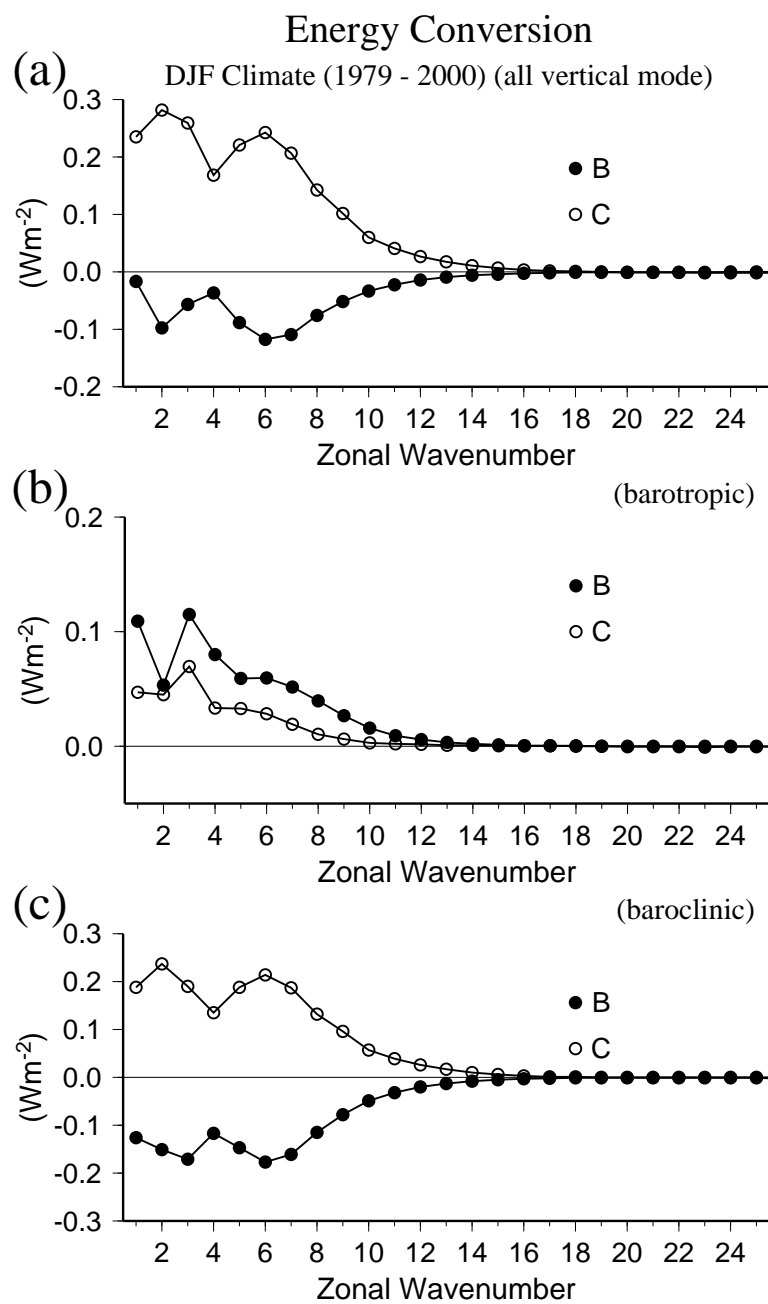


Figure 4.14. Energy Interactions in the wavenumber domain for (a) $m = 0 - 22$, (b) $m = 0$ and (c) $m = 1 - 22$. B: Interactions of kinetic energy, C: those of available potential energy.

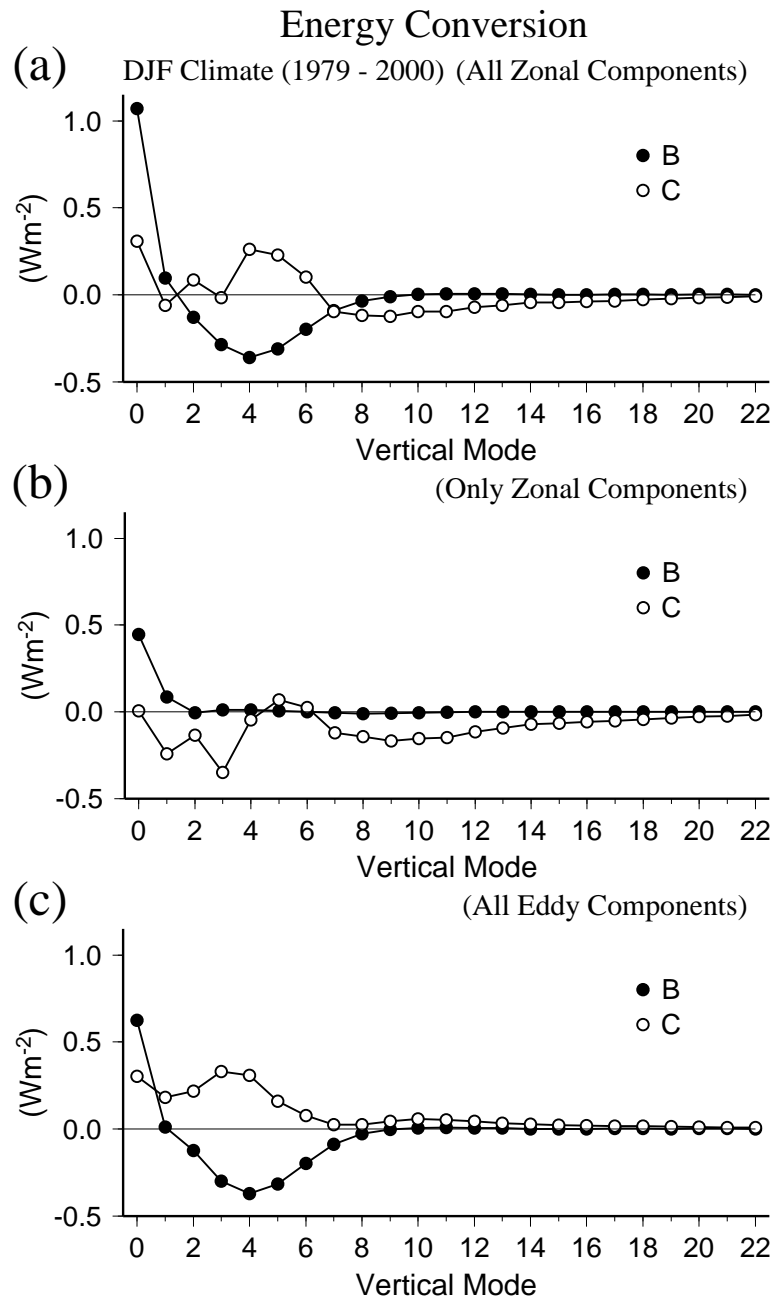


Figure 4.15. Energy Interactions in the vertical mode domain for (a) $n = 0 - 50$, (b) $n = 0$ and (c) $n = 1 - 50$.

Energy Flux (DJF climate)

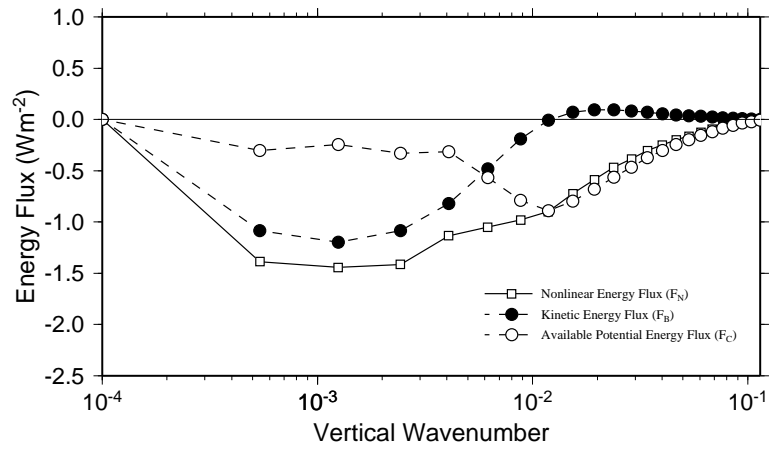


Figure 4.16. Vertical energy fluxes of kinetic energy, available potential energy, and total energy as a function of the inverse of equivalent heights.

CHAPTER V

DISCUSSION

In order to investigate the atmospheric energetics in spectral domain, it is very important what basis functions are chosen. In general, Fourier expansion is used for the basis function to zonal direction, which is constituted by trigonometric functions. The Hough vector functions are used as the meridional basis functions. Kasahara and Puri (1981) obtained the orthonormal eigensolution to the vertical structure equation. But the vertical structure functions have a large aliasing in higher order vertical modes because it is solved numerically (Fig. 2.1). In this study, we used the analytical vertical structure functions obtained by assuming a constant static stability parameter. In general, the static stability in the stratosphere is more larger than that in the troposphere, it might not be good to assume it as a constant. But the author supposes that it is better to use analytical solution than to use numerical solution, because the energy spectrum calculated with numerical solution has much aliasing in the large vertical modes (Fig. 4.9). The vertical wavelength is determined by the vertical wavenumber, however the vertical wavelength of each vertical mode is affected by the pressure of the top of the atmosphere. It should be noticed that the vertical wavelength is different at the same vertical wavenumber if the different pressure of the top atmosphere is set.

The energy spectrum in the horizontal wavenumber domain has been investigated by many researchers. The -3 power law of the energy spectrum in the horizontal

wavenumber domain has widely known. There are some theories about this -3 spectral slope in the horizontal wavenumber. Tung and Orland (2003) suggested that the energy spectrum obeys -3 power law in the inertial subrange, which has no energy source region. Kraichnan (1967) predicted a -3 power law for 2D, isotropic and homogeneous turbulence in a forward enstrophy cascading inertial subrange on the short-wave side of the scale of energy injection. In this study, the energy spectrum in the vertical wavenumber domain was investigated using the analytical vertical structure functions. It is found that the vertical kinetic energy spectrum obeys the law of -3 power of the vertical wavenumber. This -3 power spectrum can not be obtained due to the aliasing in the higher vertical wavenumber, if the numerical vertical structure functions are used. There is no theory about the -3 power law of the energy spectrum in the vertical wavenumber domain. There must be some theorem for this specific spectrum in the vertical wavenumber domain, such as 2 power law of the phase speed which was derived from Rossby wave saturation theory (Tanaka et al. 2004).

In this study, a new analysis method for energy cycle in the vertical wavenumber domain is suggested using the analytical vertical structure functions. The baroclinic-baroclinic interaction terms of kinetic and available potential energies vanish when they are summed up with all vertical modes, and the energy cycle between barotropic (mean) and baroclinic (shear) can be estimated. The calculation of interaction terms is very difficult, because these terms are affected by the boundary condition and the calculation method, and so on. The energy of the atmospheric general circulation

is mostly included in the troposphere because the density above the stratosphere is much less than in the troposphere. The half-wavelength of the vertical mode $m = 4$ is about 13.7km which is one of the baroclinic modes. This scale corresponds to the scale of the tropospheric baroclinic structure which has a opposite sign at lower troposphere and upper troposphere. The vertical modes around $m = 4$, for example $m = 3$ and $m = 5$, have similar vertical scales, so the baroclinic kinetic energy and available potential energy around the vertical mode $m = 4$ has as much energy as $m = 4$. It is suggested that the energy of the polar vortex in the stratosphere is indicated in $m = 1$ which has a large amplitude and scale in the stratosphere. The $m = 1$ of the kinetic energy receives energy by the barotropic-baroclinic interactions.

CHAPTER VI

CONCLUSIONS

In this study, the atmospheric energetics in the vertical wavenumber are analyzed. The analytical vertical structure functions are used as the basis functions in the vertical direction. The analytical vertical structure functions can be obtained by assuming the static stability parameter γ to be constant value. The energy spectrum and the energy interactions of the atmospheric general circulation are also analyzed, using the expansion in three dimensional normal mode functions. The data used in this study are JRA-25 and JCDAS from 1979 to 2007.

The vertical expansion is applied to a system of the primitive equations in consideration of the proper boundary conditions, and the kinetic energy and available potential energy equations are derived. Using this analysis method, we can examine the interactions of kinetic and available potential energies among baroclinic modes.

According to the result of the analysis in dividing the atmospheric data into vertical mean (barotropic) and its shear (baroclinic), we obtain the energy circulation of the atmospheric general circulation. This result is consistent with previous studies.

According to the result of the analysis in the vertical wavenumber domain, it is found that the baroclinic kinetic energy interacts within the baroclinic modes, and then they are transformed to the barotropic mode. The interactions for available potential energy are very small compared to that for the kinetic energy.

According to the result of the energy spectrum, the vertical energy spectrum is found to be red spectrum with characteristic spectral slopes of -3 power of the vertical wavenumber for kinetic energy. There is a marked energy peak at the vertical wavenumber 1.8266 for both kinetic energy and available potential energy. The tropospheric jet near 200 hPa may cause the secondary maximum of the kinetic energy at the vertical structure function for $m=4$, having a maximum at about 200 hPa and the opposite sign at lower troposphere. The baroclinic structure of geopotential deviation from the global mean, which has an opposite sign at low and high troposphere, may be reflected at $m=4$. The barotropic energy is mostly explained by kinetic energy, whereas the higher order vertical modes are mostly explained by available potential energy.

The result obtained in this study shows significant contrast with the vertical energy spectrum by Tanaka (1985) and Tanaka and Kung (1988), where the spectrum in the higher order vertical modes appears to be zigzag by the influence of aliasing in the vertical structure functions.

According to the result for the energy interactions, energy flows are represented from the zonal baroclinic energy to eddy baroclinic energy to eddy barotropic energy, and finally to zonal barotropic energy, as is consistent with the result by Tanaka and Kung (1988). It is found in this study using the analytical vertical structure functions that there are small but consistently negative values of nonlinear interactions of available potential energy at zonal baroclinic components in the higher order vertical modes. The result suggests that the source of available potential energy in the zonal

field is distributed in wide range of the vertical spectrum at large vertical wavenumbers. The energy source of the atmospheric general circulation is basically explained by the solar radiation, which is transformed to sensible and latent heat. The former has a peak near the surface while the latter has a peak in the mid troposphere. In order to represent the diabatic heating by the sensible heat near the surface, not only the lower order modes but also the higher order modes of the vertical structure functions are required.

The analysis of vertical energy flux shows that the energy injected at the higher order baroclinic modes by the solar radiation is transformed to lower order vertical modes, ultimately to barotropic mode.

Most of the previous 2D turbulence experiments are conducted under no energy source or at most with a point-wise energy source in order to examine the inertial subrange. Welch and Tung (1998) examined the energy slope with two-level quasi-geostrophic model, which is a baroclinic model. Basdevant et al. (1981) investigated using the barotropic nondivergent model with forcing. They obtained the -4 power spectrum with their model which has a rotation and baroclinic instability as a forcing. It is similar to our saturation theory of the Rossby wave. But they did not mention why the energy slope becomes -4 power law for the barotropic component.

In this study, the characteristics of the energy slope for the barotropic component is examined in the framework of the 3D normal mode decomposition. The energy slope of $E = mc^2$ was derived by Tanaka et al. (2004) based on the criterion of the

Rossby wave breaking. The wave breaking occurs when the local meridional gradient of the potential vorticity is negative, i.e., $\partial q/\partial y < 0$, somewhere in the domain.

In this study, it is derived that the energy spectrum for the barotropic component obeys the -4 power of zonal wavenumber, because the phase speed of the Rossby wave c can be replaced with total wavenumber, $c = -\beta/k^2$, and if we assume the isotropy for zonal wind u and the meridional wind v over the range of synoptic to short waves, the energy spectrum can be expressed as a function of n instead of k . This theoretical law of the energy slope is examined by analyzing with JRA-25.

According to the result of the analysis, the spectral slope agrees quite well with the -4 power law for the barotropic component of the atmosphere. It is, however, confirmed that the spectrum obeys the -3 power law as in previous studies for the baroclinic atmosphere. It is also found that the barotropic energy spectrum obeys the saturation theory where energy cascades up, but it does not obey where energy cascades down.

ACKNOWLEDGMENTS

First of all, I would like to express special appreciation to Prof. Hiroshi L. Tanaka, Center for Computational Sciences, University of Tsukuba, for his variable comments and encouragements. I am also thankful to Profs. F. Kimura, Y. Hayashi, A. Kitoh, K. Ueno, H. Ueda, and H. Kusaka for variable comments and suggestions. I am most grateful to Dr. Watarai in Rissho University and Dr. Matsueda in MRI-JMA for their various advice on my study. I am grateful to all other students and staff of the Climatology and Meteorology Group, the University of Tsukuba, for their comments and supports. Finally, I am most thankful to my family for their support and understanding.

REFERENCES

- Boer. G. J. and T. G. Shepherd, 1983: Large-scale two-dimensional turbulence in the atmosphere. *J. Atmos. Sci.*, **40**, 164–184.
- Basdevant, C., Legras, R. Sadourny, and M. Beland, 1981: A Study of Barotropic Model Flows: Intermittency, Waves and Predictability. *J. Atmos. Sci.*, **38**, 2305–2326.
- Ferdinand, B., 1981: Three-dimensional scaling and structure of atmospheric energetics. *J. Atmos. Sci.*, **38**, 52–68.
- Garcia, R. R., 1991: Parameterization of planetary wave breaking in the middle atmosphere, *J. Atmos. Sci.*, **48**, 1405–1419.
- Kasahara, A., 1976: Normal modes of ultralong waves in the atmosphere. *Mon. Wea. Rev.*, **104**, 669–690.
- Kasahara, A. and K. Puri, 1981: Spectral representation of three dimensional global data by expansion in normal mode functions. *Mon. Wea. Rev.*, **109**, 37–51.
- Kasahara, A., 1984: The linear response of a stratified global atmosphere to tropical thermal forcing. *J. Atmos. Sci.*, **41**, 2217–2237.
- Kraichnan, R. H., 1967: Inertial ranges in two-dimensional turbulence, *Phys. Fluids.*, **10**, 1417–1423.
- Lorenz, E. N., 1955: Available potential energy and the maintenance of the general circulation. *Tellus*, **7**, 157–167.

- Nastrom, G. D., K. S. Gage, and W. H. Jaspersom, 1984: The atmospheric kinetic energy spectrum, 10^0 - 10^4 km, *Nature*, **310**, 36–38.
- Onogi, K., J. Tsutsui, H. Koide, M. Sakamoto, S. Kobayashi, H. Hatsushika, T. Matsumoto, N. Yamazaki, H. Kamahori, K. Takahashi, S. Kadokura, K. Wada, K. Kato, R. Oyama, T. Ose, N. Mannoji and R. Taira, 2007: The JRA-25 Reanalysis. *J. Meteorol. Soc. Japan*, **85**, 369–432.
- Saltzman, B., 1957: Equations governing the energetics of the larger scales of atmospheric turbulence in the domain of wavenumber. *J. Meteor.*, **14**, 513–523.
- Sasaki, Y. K., and L. P. Chang, 1985: Numerical solution of the vertical structure equation in the normal mode method. *Mon. Wea. Rev.*, **113**, 782–793.
- Shepherd, T., 1987: A spectral view of nonlinear fluxes and stationary-transient interaction in the atmosphere. *J. Atmos. Sci.*, **44**, 1166–1178.
- Smagorinsky, J., 1963: General circulation experiments with the primitive equations. *Mon. Wea. Rev.*, **91**, 99–165.
- Stone, P., 1978: Baroclinic adjustment, *J. Atmos. Sci.*, **35**, 561–571.
- Swarztrauber, P. N. and A. Kasahara, 1985: The vector harmonic analysis of Laplace’s tidal equation. *SIAM J. Sci. Stat. Comput.*, **6**, 464–491.
- Tanaka, H.L., 1985: Global energetics analysis by expansion into three dimensional normal mode functions during the FGGE winter. *J. Meteor. Soc. Japan*, **63**, 180–200.
- Tanaka. H. L and E. C. Kung, 1988: Normal mode energetics of the general circu-

- lation during the FGGE year. *J. Atmos. Sci.*, **45**, 3723–3736.
- Tanaka, H. L., Y. Watarai, and T. Kanda, 2004: Energy spectrum proportional to the squared phase speed of Rossby modes in the general circulation of the atmosphere. *Geophys. Res. Letters*, **31**(13), 13109, doi: 10.1029/2004GL019826.
- Terasaki, K. and H. L. Tanaka, 2007a: Barotropic energy spectrum by the Rossby wavesaturation in the zonal wavenumber domain. *SOLA*, **3**, 25-28.
- Terasaki, K. and H. L. Tanaka, 2007b: An Analysis of the 3-D Atmospheric Energy Spectra and Interactions using Analytical Vertical Structure Functions and Two Reanalyses. *J. Meteor. Soc. Japan*, **85**, 785–796.
- Tung, K. K. and W. W. Orland, 2003: The k^{-3} and $k^{-5/3}$ energy spectrum of atmospheric turbulence: Quasigeostrophic two-level model simulation, *J. Atmos. Sci.*, **60**, 824–835.
- Welch. W. T. and K. K. Tung, 1988: On the equilibrium spectrum of transient waves in the atmosphere. *J. Atmos. Sci.*, **55**, 2833–2851.
- Wiin-Nielsen. A., 1962: On transformation of kinetic energy between the vertical shear flow and the vertical mean flow in the atmosphere. *Mon. Wea. Rev.*, **90**, 311–323.
- Wiin-Nielsen. A. and M. Drake, 1965: On the energy exchange between the baroclinic and batropic components of atmospheric flow. *Mon. Wea. Rev.*, **93**, 73–92.
- William, E. and Richard, C, 2005: Elementary Differential Equations and Boundary

value problems Eighth Edition, 273–279.

Žagar, N., Y. J. Tribbia, J. L. Anderson, and K. Raeder, 2008: Quantification of inertio-gravity energy in atmospheric analyses by using normal modes. Part I: intercomparison of four analysis systems. (submitted to MWR).